Design of a small-scale pico-hydro system using pumps as turbines

Gabriel Henrique Nenevê

Supervised by:

Prof. Dr. Américo Vicente Teixeira Leite

Prof. Dr. Jair Urbanetz

Bragança

2022

Design of a small-scale pico-hydro system using pumps as turbines

Gabriel Henrique Nenevê

Dissertation submitted to the School of Technology and Management of the Polytechnic Institute of Bragança, under the Double Diploma Agreement between the Polytechnic Institute of Bragança, Portugal, and the Federal University of Technology - Paraná, Brazil, to fulfill the requirements of a Master of Science Degree in Renewable Energy and Energy Efficiency.

Supervised by:

Prof. Dr. Américo Vicente Teixeira Leite

Prof. Dr. Jair Urbanetz

Bragança

2022

Dedication

I would like to dedicate my work to my dear family, who have always supported and motivated me to follow my dreams.

In loving memory of my grandmother Dulce.

"Tudo posso Naquele que me fortalece" (Fp 4:13)

Acknowledgement

First and foremost, I would like to thank God for having granted me countless blessings, knowledge, and opportunities so that I could accomplish this thesis.

Apart from myself, the success of this thesis largely depends on the encouragement and guidance of many others. I take this opportunity to express my gratitude to people who have been fundamental to the successful ending of this work.

To my parents, Marcelo and Luciane, for their endless love and efforts to always give me the best, making it possible for me to reach here.

To my siblings, Bruno and Isadora, who have always been my best friends and have been by my side when I needed.

To my grandparents, uncles, cousins and all my family for believing in me, for supporting me and for always being there, despite the physical distance.

To my Ingrid, for her encouragement, support, companionship, care, and love. For helping me improve my English language skills, and especially for helping me find purpose in difficult times.

To my supervisors, Prof. Dr. Vicente Leite and Prof. Dr. Jair Urbanetz, for their guidance, discussions, and suggestions so that I could develop this work. Also, to Prof. Batista, for his help in the experimental steps in the lab.

To my friend Bruno Zanelato, who has been with me in my academic journey since the first day of college as a great classmate and a dear friend.

To my teachers who have encouraged and instigated me to always go further. A special acknowledgement to Prof. João Marcos Varela and Prof. Rudnei Machado.

To my mentors during my internships, Luiz Melnecenko, André de Freitas, André

Frâncica, and Bruno Bytner, for all their teachings and for helping me maximize my potential both personally and professionally.

To all my long time friends, for all the moments, stories and lessons learned, making this journey unforgettable.

Last but not least, to all the people who have not been mentioned, but who contributed directly or indirectly to this work.

Abstract

New approaches to renewable energy sources and the growing interest in clean energy technologies nowadays are related to the context of the war in Europe, rising electricity prices, depletion of fossil fuel reserves, and environmental issues. Still, many European countries can develop and exploit the untapped potential of hydropower generation and take advantage of new solutions for emerging small-scale distributed generation. Regarding small-scale pico-hydro systems, many researchers have been studying to apply reversed-flow centrifugal pumps instead of conventional turbines, as they are easy to install, low cost, less complex to operate, mass-produced, and available for a wide range of head and flow rates. Notwithstanding, selecting a pump as a turbine (PAT) is not that simple since pump manufacturers do not provide performance curves for reverse operation. Therefore, based on several authors, this work designed a small-scale pico-hydro system to be implemented at the Bragança Ciência Viva Centre using two PATs, whose selection and performance prediction were carried out through an easy and reliable procedure. A solution is proposed considering three power generation levels in order to obtain high self-consumption quotas, forecasting an energy generation of 57% of the total yearly consumption. Additionally, preliminary tests were carried out in the lab, although not sufficiently conclusive, for an innovative grid connection solution using a PAT emulation system, a VFD in regenerative braking mode, protection circuits, and a PV inverter.

Keywords: Small-scale pico-hydro systems; renewable distributed generation; PATs;

Resumo

Novas abordagens em fontes renováveis e o crescente interesse pelas tecnologias de energia limpa atualmente se remetem ao contexto da guerra na Europa, ao aumento dos preços da eletricidade, ao esgotamento das reservas de combustíveis fósseis, e a questões ambientais. Outrossim, muitos países europeus podem desenvolver e se beneficiar de um potencial hidroelétrico ainda inexplorado, aproveitando novas e emergentes soluções para a geração distribuída em pequena escala. Quanto a sistemas pico-hídricos de pequena escala, muitos investigadores têm estudado a aplicação de bombas centrífugas a funcionar como turbinas (BFT), uma vez que são fáceis de instalar, de baixo custo, menos complexas de operar, produzidas em massa, e disponíveis para uma vasta gama de cota e de caudal. Contudo, selecionar uma BFT não é tão simples, posto que os fabricantes de bombas não fornecem curvas de desempenho para o funcionamento inverso. Portanto, com base em vários autores, concebeu-se um sistema pico-hídrico de pequena escala para ser implementado no Centro Ciência Viva de Bragança utilizando duas BFTs, cuja seleção e previsão de desempenho foram realizadas através de um procedimento fácil e confiável. Propõe-se uma solução considerando três escalões de geração de energia para elevadas quotas de autoconsumo, prevendo uma geração de energia de 57% do consumo total anual. Ademais, foram realizados testes preliminares no laboratório, ainda que não suficientemente conclusivos, de uma solução inovadora de ligação à rede a partir de um conversor de frequência em modo de travagem regenerativa, circuitos de proteção, e um inversor fotovoltaico.

Palavras-chave: Sistemas pico-hídricos de pequena escala; geração distribuída renovável; BFTs;

Contents

List of Tables

List of Figures

Acronyms

AC Alternating Current.

BEP Best Efficiency Point.

BTE *Baixa Tensão Especial*.

CCVB *Centro Ciência Viva de Bragança*.

CFD Computational Fluid Dynamics.

DC Direct Current.

DG Distributed Generation.

ECSITE European Network of Science Centres and Museums.

IGBT Insulated Gate Bipolar Transistors.

IPB Instituto Politécnico de Bragança.

MPPT Maximum Power Point Tracking.

NPSH Net Positive Suction Head.

PAT Pump as Turbine.

PHES Pumped Hydro Energy Storage.

PMSG Permanent Magnet Synchronous Generator.

PRV Pressure-Reducing Valve.

PV Photovoltaic.

PWM Pulse-Width Modulation.

SEIG Self-Excited Induction Generator.

VFD Variable Frequency Drive.

WDN Water Distribution Network.

Symbols

C_H	Head ratio
C_Q	Discharge ratio
C_η	Efficiency ratio
f	System frequency
g	Gravity acceleration
H	Head pressure
H_{bP}	Pump head at BEP
H_{bT}	Turbine head at BEP
H_{site}	Head at the site
h	Dimensionless parameter for the head
$H_{L,N}$	Turbine head in runaway condition
H_W	Turbine head in zero-speed condition
n	Rotational speed
n_s	Specific speed
n_{sP}	Specific speed of the pump
n_{sT}	Specific speed of the turbine
N_s	Synchronous speed

P	Power
P_O	Generated electrical power
P_h	Hydraulic power
p	Dimensionless parameter for the power
p_m	Number of magnetic poles of the machine
Q	Flow rate
Q_{bP}	Pump flow rate at BEP
Q_{bT}	Turbine flow rate at BEP
Q_{site}	Flow rate at the site
$Q_{L,N}$	Turbine flow rate in runaway condition
Q_W	Turbine flow rate in zero-speed condition
q	Dimensionless parameter for the flow rate
η	Efficiency
η_g	Generator efficiency
η_t	Turbine efficiency
η_{bP}	Pump efficiency at BEP
η_{bT}	Turbine efficiency at BEP
η_{max_T}	Maximum efficiency in turbine mode

Chapter 1

Introduction

Energy generation and consumption are essential factors in the advancement of society. Power generation solutions have been increasingly developed to meet the growing energy demand. The availability of electricity is a prime necessity today as it can improve the quality of life in many ways, even though a considerable percentage of the world still does not have access to electricity [1].

Fuels still supply a significant part of the energy demand, representing emissions in large quantities of greenhouse gases and resulting in increasing weather changes, severe health problems, sea-level rise, and changes in the ecosystem. The energy mix cannot depend on fossil fuels anymore, making room for developing renewable sources in various contexts, enabling several benefits for the environment, society, and economy [2, 3].

The context of the war in Ukraine further aggravates the rising electricity prices and presents a massive challenge considering the EU's dependency on Russian natural gas – spotlighting the market of small-scale renewable energy generation. Gathering resources, knowledge base, and determination, it is possible to turn the crisis into an opportunity [3, 4].

1.1 Motivation and challenges

New approaches to renewable energy sources and the environmental issues of fossil fuels have increased the interest in clean energy technologies. Intensive exploration of alternatives and renewable energy resources are currently being conducted worldwide [5]. In this respect, distributed generation (DG) is becoming part of the strategic plans of most countries as it produces on-site highly reliable and good quality electrical power, offering environmental, technical, and economic advantages [6, 7].

Regarding the European region, many countries can still develop and exploit the untapped potential of hydropower generation, which needs to expand further to enable clean energy transition and limit the global temperature rise in the following decades [8]. Large-scale hydropower plants have lower electricity generation costs but are usually related to large dams and present a matter of distributing or transmitting the energy produced. By contrast, on a small scale, hydropower exploits the hydro potential without significant damming, being an environmentally benign energy option available [9, 10].

Furthermore, conventional turbines and generators can neither be produced locally nor mass-produced, which is why it is difficult, time-consuming, and costly to develop turbines for a specific site in a low-capacity range [11]. Alternatively, many researchers have been studying the replacement of these turbines with reversed-flow centrifugal pumps in small-scale hydropower systems. They are easy to install, low cost, less complex to operate, mass-produced, and available for a wide range of head and flow rates [11]. Integrating mature technologies, which are widely available at competitive prices, it is possible to reach both remote areas and places where the power grid is accessible [7].

Notwithstanding, selecting a pump to run as a turbine (PAT) is not that simple. Since pump manufacturers do not provide performance curves for reverse operation, predicting pump behavior and performance is needed, but it requires complex and expensive laboratory equipment to be obtained. An easy and reliable way for predicting PAT performance is still an open issue [12].

Different types of generators and connection strategies can be applied to the interface

between the turbine and the power grid. Generally, a commercial pump is sold with a three-phase asynchronous motor as a prime mover, which can also operate as a generator. The induction machine can compete with other technologies for a small-scale generation. However, manufacturers' catalogs only mention motor efficiency values [13].

Connecting the generator directly to the power system may imply large inrush currents and voltage drops, and grid connection approaches aim to avoid such undesirable effects. Moreover, integrating renewable sources in unconventional ways has proven viable and has been studied recently. Developing reliable and cheap conversion systems, based on mature technologies, is necessary to allow these solutions to be exploited cost-effectively [14, 15].

The Bragança Ciência Viva Centre (CCVB), next to the Fervença river, is a smart and eco-efficient building with a conventional micro-hydro system, which has recently experienced some difficulties in its operation [16, 17]. In the context of small-scale hydropower plants, there is an opportunity to study the new approaches, taking advantage of the available water resource and being an alternative to the existing infrastructure.

1.2 Objectives

This work aims to design a small-scale pico-hydro system based on PATs at the CCVB, in order to exploit the available hydroelectric potential on a self-consumption basis, as an alternative to the existing out-of-service micro-hydro system.

The specific objectives of this work are listed as follows:

- Review the literature on small-scale renewable energy generation, focusing on distributed generation and pico-hydro systems;
- Study the application of PATs in the context of small-scale pico-hydro systems, proposing a method to select and predict the operation for a given site;
- Study grid connection strategies suitable for small-scale hydropower plants based on PATs;

- Apply the selecting procedure proposed and predict the performance parameters for the context of the CCVB;
- Forecast renewable energy generation in the applied context, discussing benefits, drawbacks, and requirements of the system;
- Test innovative grid connection approaches within small-scale pico-hydro systems.

1.3 Structure of the Thesis

- Chapter 1: Introduction
  – Contextualization of the growing interest in renewable resources and distributed generation, introducing opportunities to investigate and develop alternatives in this area, especially concerning small-scale hydro systems.
- Chapter 2: State of the Art
  – Literature review on renewable energy generation mainly focused on pico-hydro systems using PATs, presenting a procedure to select and predict their performance and also approaching grid connection strategies.
- Chapter 3: Site characterization
  – Description of the context of the CCVB, consumption data and site parameters, presenting the information required to develop a design project.
- Chapter 4: Application and Results
  – Application of the State of the Art within the context presented, reporting the results to be discussed.
- Chapter 5: Conclusion
  – Synthesis of the work and suggestions for future work.

Chapter 2

State of the Art

Power generation solutions are sought after to meet the growing energy demand. The energy mix cannot depend on fossil fuels anymore, making room for the development of renewable sources in various contexts, enabling several benefits for the environment, society, and economy. This chapter reviews the current status of electricity demand and generation as well as approaches to small-scale generation plants and grid connection strategies to be applied in the context of this work.

2.1 Small-scale renewable energy generation

This section will focus on the context of electricity demand and generation and how small-scale distributed generation and especially small-scale pico-hydro systems can integrate into that scenario.

2.1.1 Current status of electricity demand and generation

Electricity availability is a prime necessity these days, as it can improve the quality of life in many ways. Nevertheless, 9.5% of the world had no electricity access in 2020 – concerning either electricity supply, safe cooking facilities, and a required minimum level of consumption [1] –, as Figure 2.1 shows.

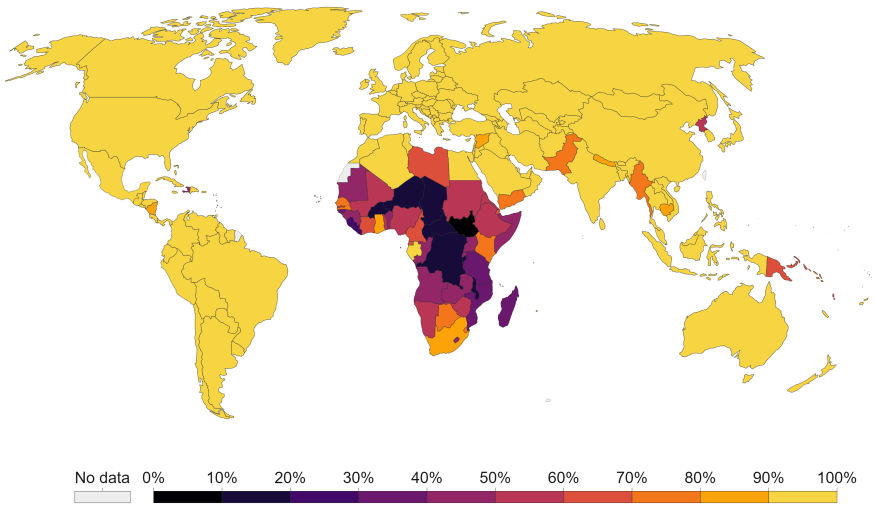

Figure 2.1: Electricity access, 2020. Source: Our World In Data [1].

Reducing this amount is a great challenge, considering that some places deprived of electricity are complicated to reach, and the cost of electricity from different power generation sources can vary [2].

In addition, fossil fuels still supply a significant part of the energy demand, which continues to present exponential growth, as well as the rate of civil and industrial growth and technological advances. This scenario represents emissions in large quantities of greenhouse gases during the combustion process, resulting, e.g., in increasing weather changes, severe health problems, sea-level rise, and changes in the ecosystem. On the other hand, fossil fuel reserve depletion has accelerated research in renewable energy, intending to make energy available at low cost and higher efficiency [2, 3].

Rising fossil fuel prices and Europe's ambition to reduce its energy import dependency spotlight the market of small-scale electric energy generation units. Based on these facts, many nations and governments started implementing energy strategies and policies to reduce environmental impacts and develop new and efficient renewable technologies, needing to overcome many challenges and barriers. For many years, the energy market was dominated by fossil energy resources, setting up regulations and policies and hindering the deployment of renewable energy resources. Regulatory and policy support is

necessary to change this scenario. Energy incentives (fixed feed-in tariffs, quotas, energy bids, and auctions), exemption from taxes, importation duties and customs, low-interest rates, and energy credit; such measures can enable renewable energy projects [3, 13].

Replacing existing power plants with renewable ones is expensive, as well as the cost of electricity produced from renewable energy. So it still requires subsidy policies to be competitive with traditional sources, such as facility investment subsidy for replacement and electricity price subsidy. Furthermore, these sources require high-level skilled labor with specific expertise to install, commission, operate, and maintain their facilities, which is another challenge for deploying renewable energy projects [3].

One must consider that the context of the war in Ukraine further aggravates the rising electricity prices and presents a massive challenge considering the EU's dependency on Russian natural gas – which has become unreliable and expensive. The war will reinforce speeches in favor of other renewable energy sources and foreground them, as happened in the late 2000s when countries began to consider renewable energy as a measure of energy independence. Gathering resources, knowledge base, and determination, it is possible to turn the crisis into an opportunity. Nevertheless, if uncoordinated or mismanaged, this crisis may worsen [4].

2.1.2 Small-scale distributed generation

As mentioned, new approaches to renewable energy sources and the environmental issues of fossil fuels have increased interest in clean energy technologies. Intensive exploration of alternatives and renewable energy resources are currently being conducted worldwide [5]. During the last decade, global energy generation from renewable sources jumped from 4,401 TWh per year in 2011 to 7,931 TWh in 2021 [18], representing an increase of more than 80%, as shown in Figure 2.2.

In this respect, distributed generation (DG) is becoming part of the strategic plans of most countries as it produces on-site highly reliable and good quality electrical power, offering environmental, technical, and economic advantages [6, 7]. It refers to small and

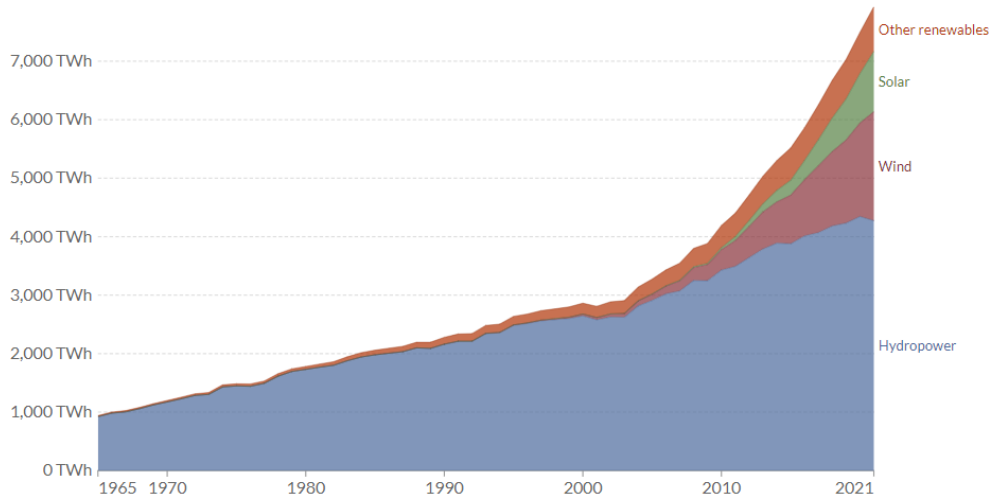

Figure 2.2: World renewable energy production. Source: Our World In Data [18].

medium-sized power plants located near electricity users and is becoming increasingly important in the global energy supply systems. Renewable energy DG technologies has the potential to mitigate congestion on transmission lines, reduce the impact of electricity price fluctuations, increase energy security, and provide greater stability to the power grid [19].

Integrating renewable sources in unconventional ways has proven to be viable and has been studied recently. DG emerges as an interesting solution to electrify remote areas and also to make buildings more sustainable. While grid-connected small-scale PV systems are widespread, small-scale hydropower systems are promising and have potential – especially very small-scale [7].

Pico-hydro systems – under 5 kW –, for example, can be implemented with low-power wind generators connected to the grid through a PV inverter [20]. Moreover, developing reliable and cheap conversion systems, based on mature technologies, is necessary to allow these solutions to be exploited cost-effectively [15].

2.1.3 Small-scale hydropower systems

Within the context of renewable generation, hydropower appears as the cheapest among other sources. It generates electricity by using a turbine to convert the energy

of falling water to mechanical energy, and generators coupled to these turbines to convert from mechanical to electrical energy [2, 9]. As the largest source of renewable electricity globally, hydropower generates more electricity than all other renewable energies combined. By 2021, it generated around 54% of all energy from renewable sources [18].

Nevertheless, hydropower capacity needs to expand further to enable clean energy transition and limit the global temperature rise in the next decades. In 2019, renewable sources accounted for only 11.4% of global primary energy, so they must comprise a much larger proportion of the world's energy mix by 2050. Rapid electrification in all sectors and the increasing world population show that the electricity demand will increase in the coming decades. Thus, hydropower, wind, and solar will all have to increase significantly to meet this demand [21]. Regarding the European region, many countries can still develop and exploit the untapped potential of hydropower generation [8].

Despite large-scale hydropower plants having even lower electricity generation costs, there is a matter of distributing or transmitting the energy produced, which may not be economical. Besides that, hydroelectricity is usually with large dams. However, hydropower on a small scale is the exploitation of hydro potential without significant damming, being in most cases close to the consumer and run-of-river plants – which do not have the same kinds of adverse effect as the large hydro. Therefore, small-scale hydropower is one of the most environmentally benign energy options available [9, 10], even more so in the mentioned context of DG. The classification of hydropower plants will be shown in the next section.

Pico-hydro systems can provide electricity where there are many isolated rural communities and villages near streams and rivers. Moreover, it is an economical power source as it has very low construction costs and a short pay-back time [11]. Especially concerning remote villages where grid supply is not feasible, standalone hydropower plants can also be a very attractive solution [2, 9].

However, it can become expensive if conventional turbines and generators are applied as they can neither be produced locally nor mass-produced [11]. Turbine manufacturers do not manufacture turbines in smaller capacities. Therefore, it is difficult, time-consuming,

and costly to develop turbines for a specific site in a low-capacity range. The cost of electromechanical components in small-scale systems is relatively high so solutions are being sought to lower this cost [22]. Figure 2.3 shows the differences in cost distribution between large and micro hydropower plants.

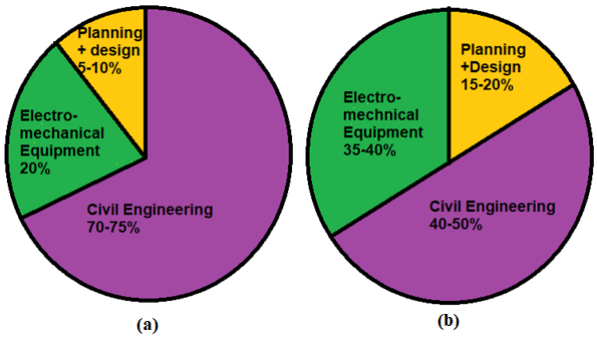

Figure 2.3: Cost distribution: (a) Large and (b) Micro hydropower plants. Source: Aidhen et al. [2].

As a solution, many researchers have been studying the replacement of these turbines with reversed-flow centrifugal pumps in small-scale hydropower systems as they are available for a wide range of head and flow rates. In addition, they are easy to install, low cost, less complex to operate, mass-produced, and available for various standard sizes and including spare parts [11]. These systems can take advantage of the integration of mature technologies, which are widely available at competitive prices, to reach both remote areas and places where the power grid is accessible [7]. The next section will discuss the above mentioned solution in more detail.

Water distribution networks (WDNs) have been in evidence as an another attractive area for applying small-scale distributed hydro generation. In this context, pressure reducing valves (PRVs), which waste a potentially recoverable hydraulic head, are replaced by pumps running as turbines to achieve both effective pressure control and a throttling energy recovery [23].

Finally, hydropower plays an important role in the energy mix, but clearly, there is still enormous potential to be tapped. Pico-hydro power systems are based on cheap, reliable, and mature technologies, enabling a widespread exploitation of small rivers and

shallows reservoirs – being even more dispatchable than solar and wind systems and the most cost-effective way to provide electricity [20].

The following section will review hydraulic machines from conventional to unconventional options, which will be further analyzed and proposed in this work.

2.2 Hydraulic machines

Conventional and well-known hydraulic turbines, such as Pelton, Francis, and Kaplan, will be presented first and briefly. Then, newer solutions and alternatives to these turbines will be introduced and compared in order to better suit small-scale applications – specifically, centrifugal pumps running as turbines.

2.2.1 Hydraulic turbines

An overview of hydraulic turbines follows. First, a hydro-turbine transforms the potential energy from a head of water into mechanical work, which can drive an electricity generator or other machinery. This process is made by various types and sizes of turbines in different forms and applications. Hydropower plants vary from very small-scale to large, and their classification is shown in Table 2.1. The hydraulic efficiency of large turbines reaches 80 to over 90%, while smaller ones are generally in the 60 to 80% range [10]. For a particular site, the height of standing water – the so-called head –, and the flow rate – the volume of water per time –, base the selection of a turbine for a project [24, 25].

There are impulse and reaction turbines. The former generally uses the velocity of the water to move a runner, discharging the water at atmospheric pressure. An impulse turbine is generally suitable for lower flow rate and larger head applications. The latter, on the other hand, generates power from the combined forces of pressure and moving water, ranging from radial flow turbines to axial or propeller types. A reaction turbine is generally used for sites with lower head and higher flow rate. Rotational speed also varies among the different types [24, 25].

Table 2.1: Classification of hydropower plants [9].

Type	**Capacity**
Large-Hydro	P >100 MW
Medium-Hydro	15 <P <100 MW
Small-Hydro	1 <P <15 MW
Mini-Hydro	100 kW <P <1 MW
Micro-Hydro	5 <P <100 kW
Pico-Hydro	P <5 kW

Given this wide range of combinations of head, flow and rotational speed, the concept of specific speed is introduced. By correlating design and operating parameters, it is useful for comparison and selection purposes [24]. Specific speed does not depend on the size of the turbine, it only characterizes the performance relating the output power of the turbine to its running speed and the head across it [10]:

$$n_s = \frac{n\, P^{0.5}}{H^{1.25}} \tag{2.1}$$

where: n_s is the specific speed of the turbine, n is the turbine speed [rpm], P is the shaft power [kW], and H is the pressure head across the turbine [m].

The three main types of hydropower turbines are Pelton, Francis, and Kaplan (Figure 2.4) – whose names pay tribute to their inventors: Lester Allan Pelton, James Francis, and Viktor Kaplan, respectively. Other common types, such as crossflow, tubular, or Turgo, will not be described.

The Pelton turbine, invented in the 1870s, is a pure impulsive turbine, generally used for very high heads and low flows. It works by converting the entire pressure head to speed through free jets discharging water into an aerated space and impinging on the buckets of a runner. Since it operates at atmospheric pressure, draft tubes are not required. The efficiency of this turbine is around 92% [24, 25].

As the first modern hydropower turbine, invented in 1849, the Francis turbine is a

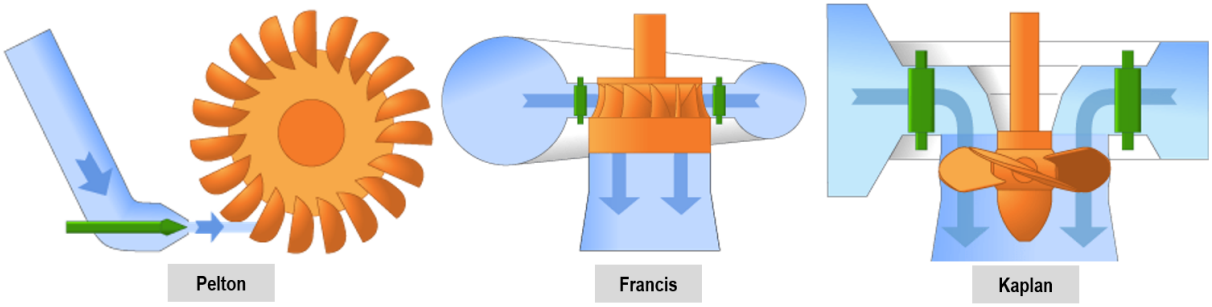

Figure 2.4: Main types of hydropower turbines. Source: WPTO [25].

reaction turbine. It is a radial flow turbine, where guide vanes are disposed all around and feed water radially to the runner. Then, after flowing radially inwards, the water is turned by the runner blades and discharged axially into the draft tube. Machine output is controlled by varying the angle of these vanes so that the water is evenly distributed to them by a spiral casing. Both horizontal and vertical orientations can be employed, and this type is commonly used for medium heads and flow rates. The maximum efficiency of this turbine is 94–95% [24, 25].

Finally, the Kaplan Turbine, invented in 1919, is also a reaction type, but it is an axial turbine. In other words, the water flows through the runner in an axial direction. Its spiral casing and guide vanes are similar to the Francis turbine. However, the water turns in an axial direction before meeting the runner, which resembles a ship's propeller. It has pitch-adjustable blades, optimizing the performance and maintaining efficiency for a wider range of operation than the Francis type. The maximum efficiency of this turbine is about 94% considering large machines [24].

Figure 2.5 presents different applications of turbines according to head and flow rate, which can be used for a preliminary selection.

One can note that there is an almost empty area for turbine selection in small-scale pico-hydro systems. As mentioned earlier, it is difficult, time-consuming, and costly to develop turbines at smaller capacities and for specific locations. To fill this void for low head and flow rates, making the implementation of pico-hydro systems more feasible, the use of pumps as turbines instead of conventional turbines will be presented next.

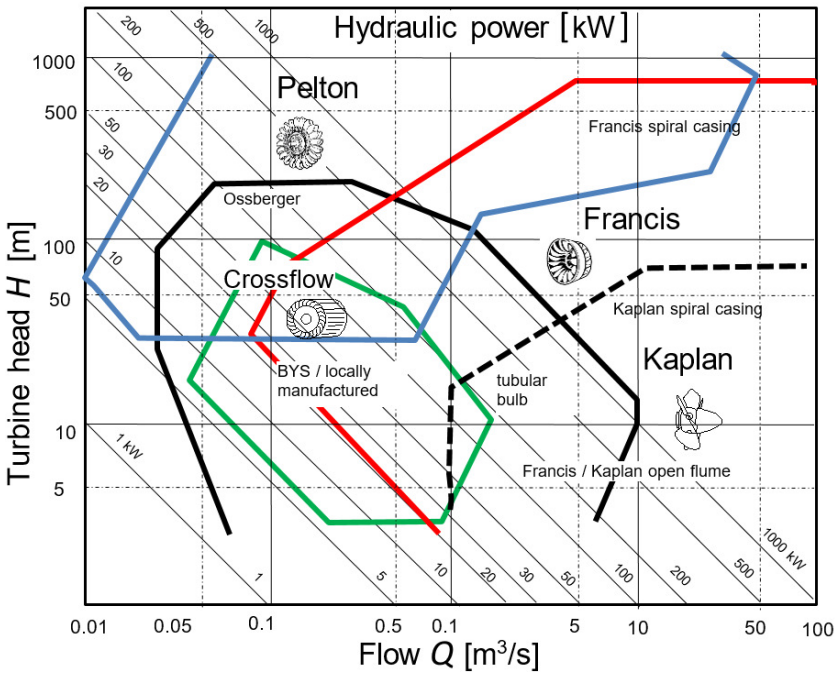

Figure 2.5: General range of application of different turbine types. Source: Barbarelli et al. [26].

2.2.2 Pumps

Turbines and pumps have the same basic hydraulic theory. However, while turbines convert the potential energy of a water head into mechanical work, and – subsequently – generate electrical power, pumps have an antagonistic operation mode. A centrifugal pump, for instance, is a turbomachine that moves water (or a fluid) by transferring rotational energy from a driven rotor – called impellers – whose shaft is coupled to a motor. Its main characteristic is that all pressure and energy differences related to the hydrodynamic process are proportional to the square of the circumferential rotor speed [27, 28].

In addition, turbines operate under variable head and flow conditions, while pumps are usually designed for one particular duty point, which must match their maximum efficiency point. For this reason, pump operation does not require guide vanes or a regulating device [28].

A centrifugal pump, according to Gülich [27], "is essentially composed of a casing,

a bearing housing, the pump shaft and an impeller. The liquid to be pumped flows through the suction nozzle to the impeller. The overhung impeller mounted on the shaft is driven via a coupling by a motor". Different pump types – with different combinations of impellers, diffusing elements and inlet casings – are available for specific performance and application requirements. Single-stage, single-entry pumps with volute casings are by far the most common pump type (Figure 2.6). Radial pumps of this type are common in many branches of industry, such as water supply, sewage, chemical processing, and power plants [27].

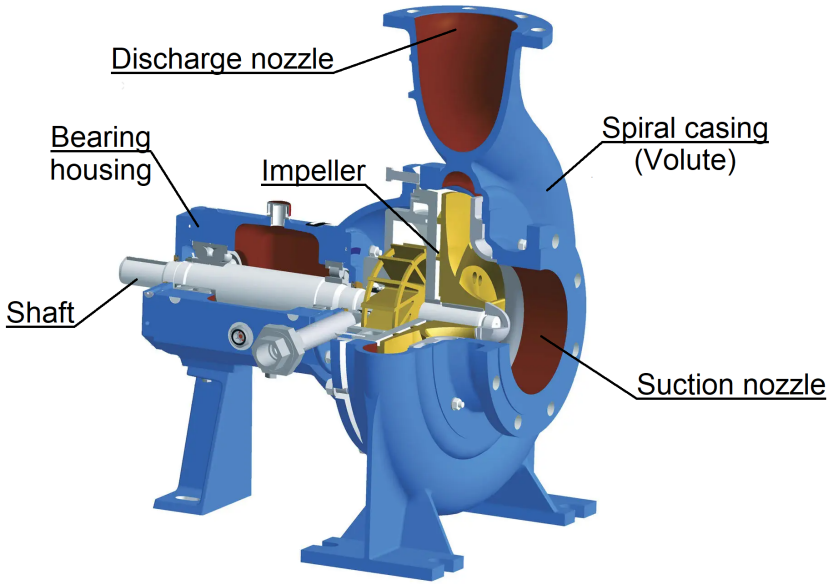

Figure 2.6: Single-stage volute centrifugal pump. Adapted from: Andritz [29].

It is worth mentioning that rotational fluid machines are reversible so that a pump can run as a turbine, despite differences in performance and hydraulic losses. Plus, in pump mode, energy transfer is determined by the shape of the vanes at the impeller outlet, while in turbine mode, it is determined by the shape of the pump casing. Although any type of pump can work as a turbine, standard centrifugal and mixed flow pumps are most commonly used for this application, as they entail lower costs than axial flow pumps [28].

2.2.3 Pump as Turbine (PAT)

As written above, hydropower is clean and the cheapest among renewable energy sources, which has different types and capacities, from pico-hydro (< 5 kW) to large-hydro (> 100 MW). Under 5 kW, it is easy to operate and maintain and has a low initial cost as construction of the dam is not required [2, 9]. Plus, using a pump as a turbine in pico-hydro systems represents significant equipment cost savings regarding custom-made turbines for a particular site [2, 9].

Besides differences in construction, as Figure 2.7 shows, conventional turbines, e.g., Pelton, Francis, and Kaplan, are expensive compared to using a pump as a turbine – also popularly called PAT. Operating as a turbine, the pressure in the pump inlet nozzle becomes greater than that in the outlet nozzle, so that the water flows in the guide wheel to the outer diameter of the runner – the terms "diffuser" and "impeller" can be respectively replaced by "runner" and "guide wheel" for this application. In this case, the pump rotates reverse, while the motor operates as a generator. A inverted flow centrifugal pump can be applied as it is cheaper, mass-produced, readily available – for a wide range of heads, flows, and sizes –, and simpler in construction and maintenance. It has easy installation, needing less space and using standard pipe fittings, besides having a direct drive arrangement – representing low friction losses [2, 9, 27].

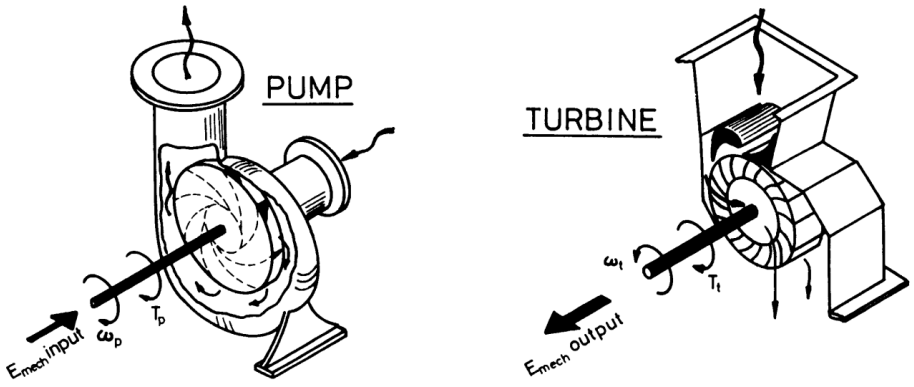

Figure 2.7: Difference between pumps and turbines. Source: Chapallaz et al. [28].

Further uses for PATs include pumped hydro energy storage (PHES) stations, energy recovery in water distribution systems (WDN), reverse osmosis systems, sewage systems,

and pressure-reducing valves (PRVs) in existing pipelines – for water purifier plants or irrigation tanks. Even in these examples it is possible to exploit the available water flow rate and pressure drop by means of a PAT [9, 12].

One must also take into account the type of pumps that are suitable as turbines based on head and flow, as it is shown in figure 2.8. It is also possible to note, as mentioned, that PATs fill the area of this graph that the conventional turbines do not, making it feasible to implement small-scale systems.

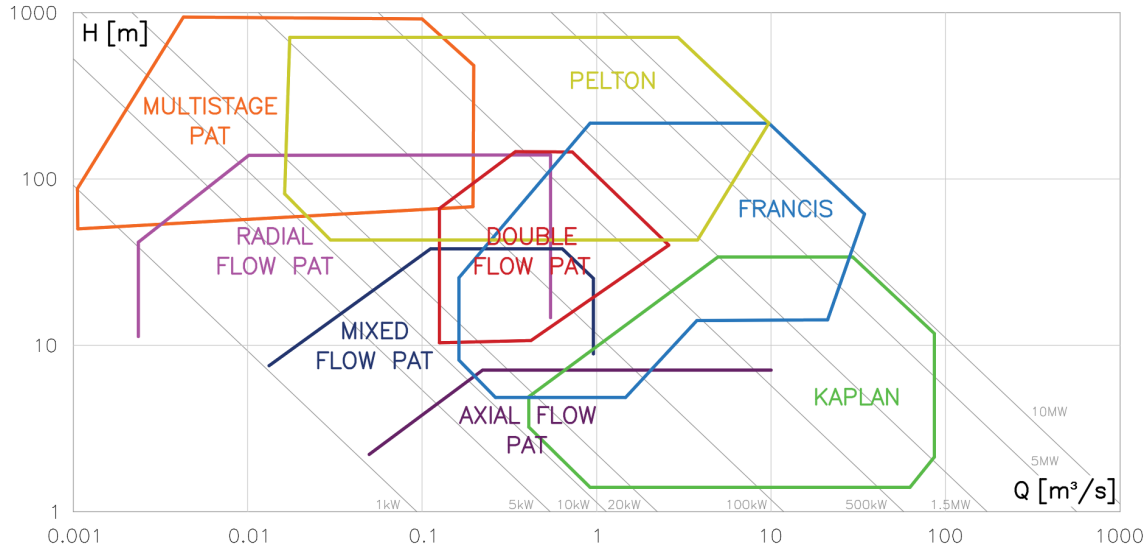

Figure 2.8: Typical operating ranges of turbines and PATs. Adapted from: Barbarelli et al. [26] and Stefanizzi et al. [23].

2.3 Design of small-scale hydropower systems using a PAT

Selecting the pump for a particular site and poor part-load efficiency in turbine mode are significant concerns of using centrifugal pumps for this application. Since pump manufacturers do not provide performance curves for reverse operation, predicting pump behavior and performance is needed, but it requires complex and expensive laboratory equipment to be obtained. Hence, selecting the pump for turbine mode is challenging

[2, 10]. This section aims to describe the process of selecting a PAT and predicting its performance curves.

First of all, it is possible to quickly estimate the system output power from the available head and flow rate using the follow equation:

$$P_o = \eta_g \cdot P_h = \eta_g \left(\eta_t \cdot g \cdot H \cdot Q\right) \tag{2.2}$$

where: P_O is the generated electrical power [kW], η_g is the generator efficiency [%], P_h is the hydraulic power [kW], η_t is the turbine efficiency [%], g is the gravity acceleration [m/s^2], H is the head [m], and Q is the flow rate [m/s^3].

According to Aidhen et al. [9], turbine efficiency and generator efficiency values can be estimated as 78 and 77%, respectively, in case of manufacturers do not provide this information. Concerning generator efficiency for standard 2-pole and 4-pole low-voltage three-phase machines, manufacturers have recently presented better efficiency values for higher efficiency machines (IE3 and IE4), with values from 85% for rated power greater than 1 kW [30].

Pipe parameters and flow determine energy losses in the pipe due to friction, which depends on the pipe's diameter and length, the pipe material – such as iron and steel –, the volumetric flow, and a certain coefficient of flow. Friction also causes additional losses in fitting, curves and valves, which are added to pipe head loss to obtain the full head loss. The pipe diameter must be selected so that the ratio of head loss to total head is between 10 and 20% [9].

Researchers have studied PAT performance using theoretical methods, numerical analysis, and experimentation. It has been observed that the efficiency in pump and turbine mode is similar for an operation close to the best efficiency point (BEP) – where the head and flow values reach maximum efficiency. However, different from pump operation, the BEP in turbine operation is close to the flow rate of shockless entry [2, 27].

Theoretical methods for PAT performance prediction are based on pump mode BEP and specific speed, proposing head and discharge correction factors. These correlations

assist in predicting head and flow in turbine mode near BEP. However, they are not necessarily accurate – some with errors of more than ±20% – and cannot be applied to all types of centrifugal pumps with different ranges of head and flow [2].

Many computational fluid dynamics (CFD) software programs have been developed recently, allowing simulations and the study of design changes, as well as saving costs and time. It is worth considering that leakage and friction losses may not be accounted for in the CFD analysis, providing higher efficiency than that obtained in an actual situation [2].

An easy and reliable way for predicting PAT performance is still an open issue. Since the geometry of the pump is hardly ever available and 3D codes are too onerous for the precision they give, it is necessary to develop simpler models applicable to select a PAT for any situation where flow rate and pressure drop are available [12].

Barbarelli et al. [26, 12] worked on a method that prioritizes this easiness through experimental and theoretical activities concerning 27 different pumps. In this same context, Pérez-Sánchez et al. [31] also presented a new approach, based on a larger sample of 181 different pumps. It resulted in statistical methods with polynomials to predict the performance curves from characterizing the pumps and defining correlation factors. The procedure is composed by preliminary selection, performance calculation, and definitive selection, through an iterative process.

2.3.1 Selection of a PAT

The flow chart presented in Figure 2.9 summarizes the PAT selecting procedure that will be further described.

The selection of a PAT for a given site usually starts from conversion factors: the discharge ratio (C_Q) and the head ratio (C_H). C_Q corresponds to the ratio between the capacity of the turbine (Q_{bT}) and that of the pump (Q_{bP}), at best efficiency point, while C_H between the head of the turbine (H_{bT}) and that of the pump (H_{bP}), also at BEP. Besides of these, some authors also present the efficiency ratio (C_η) as a third conversion

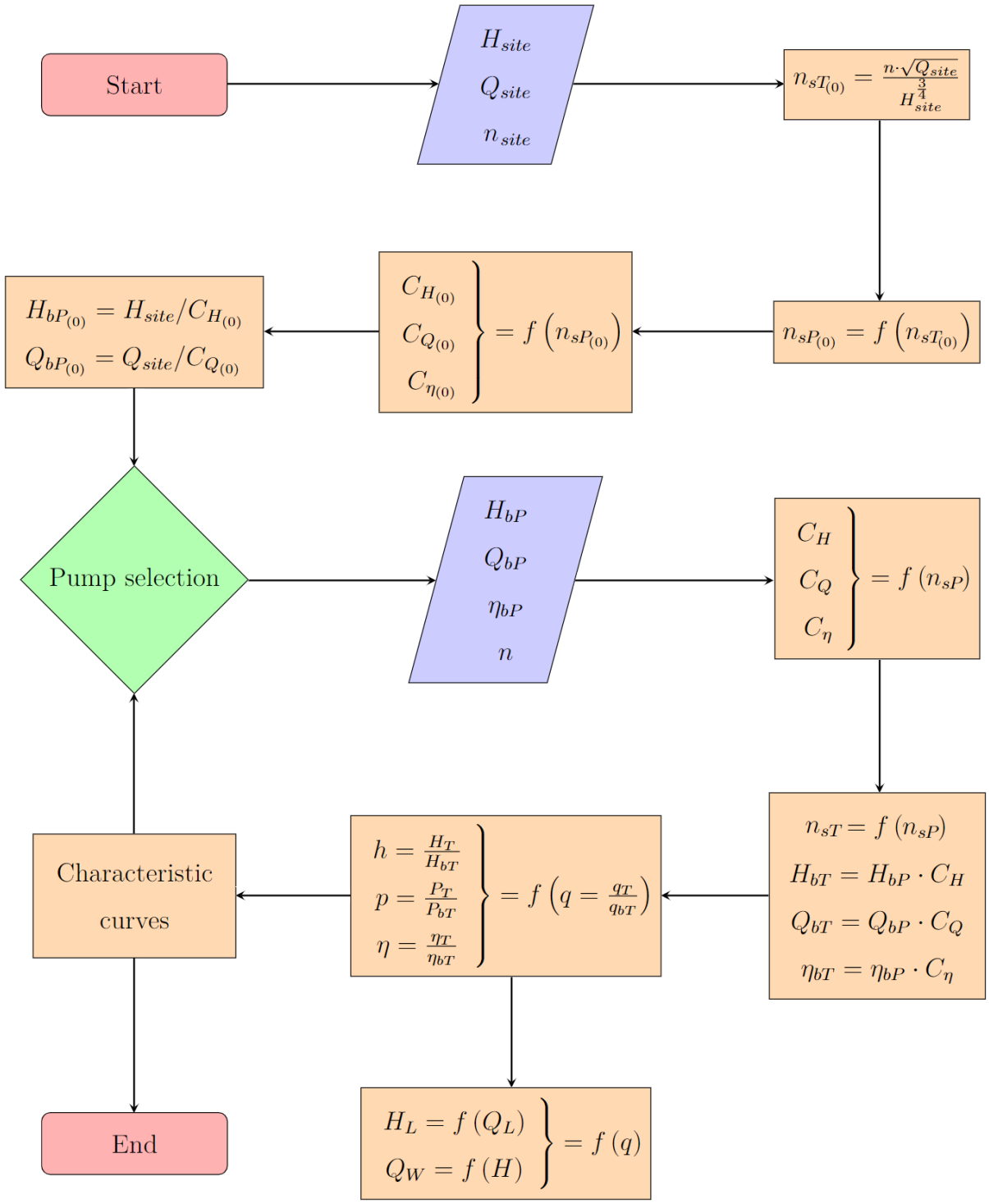

Figure 2.9: PAT selecting procedure.

factor. The representation of these factors may vary among different authors [12, 32].

$$C_Q = \frac{Q_{bT}}{Q_{bP}} \tag{2.3}$$

$$C_H = \frac{H_{bT}}{H_{bP}} \tag{2.4}$$

$$C_\eta = \frac{\eta_{bT}}{\eta_{bP}} \tag{2.5}$$

In order to characterize the pump in turbine mode, the main curves required in this process are the head-discharge curve (Q-H) – usually considering runaway and zero-speed situations – and the efficiency curve (Q-η), according to Figure 2.10.

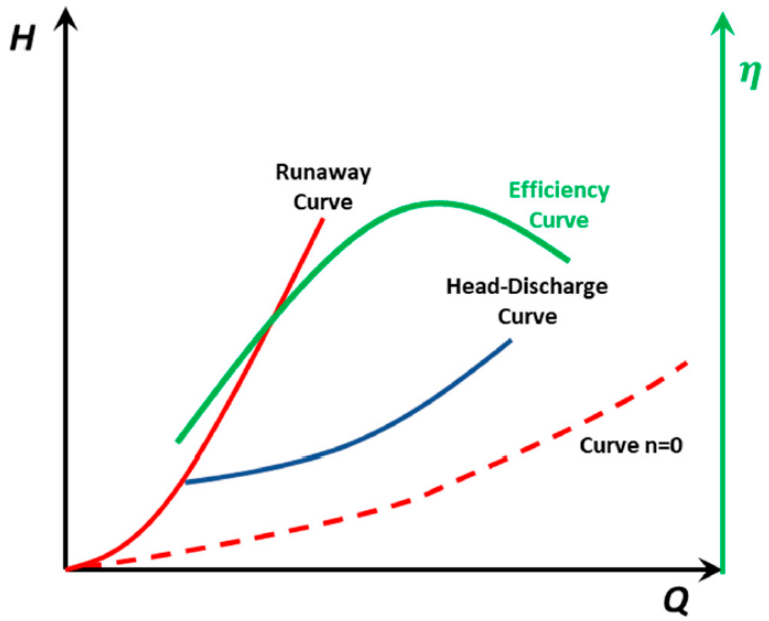

Figure 2.10: Characteristic curves of a PAT. Source: Pérez-Sánchez et al. [31].

Furthermore, authors correlated these factors to different parameters and compared the results for a large sample of pumps. For instance, Gülich [27], Childs [33], Stepanoff [34], Sharma [35], and Alatorre-Frenk [36] linked them to the BEP of the pump; Hancock [37] to the BEP of the turbine; Schmield [38] to the hydraulic efficiency of the pump; and Grover [39] and Lewinsky-Kesslitz [40] to the specific speed of the turbine. This parameter, which can be used to define the impeller typology for single suction machines,

is calculated slightly differently than in the last section:

$$n_s = \frac{n\, Q^{0.5}}{H^{0.75}} \tag{2.6}$$

where: n_s is the specific speed of the machine – either in pump (n_{sP}) or turbine mode (n_{sT}) –, n is the rotational speed [rpm], Q is the flow rate [m^3/s], and H is the head [m].

According to the specific speed of the pump n_{sP}, the typology of the machine varies to cover a wide range of powers and, as a consequence, flow rates and heads. From 10 up to 50, the shape of the impeller is of radial flow type; between 50 and 150, the impeller has mixed flow; and between 135 and 320, it has axial flow [12].

With this, it is emphasized that some uncertainty is always related to the prediction, since the machine design varies the losses and, consequently, the operating point. Statistical correlations are not able to consider the actual geometric properties of the machines. [27, 31].

First of all, for a preliminary pump selection, the specific speed required by the site is set to match the specific speed of the later chosen PAT – when it operates at BEP:

$$n_{site} = n_{sT_{(0)}} = \frac{n\, Q_{site}^{0.5}}{H_{site}^{0.75}} \tag{2.7}$$

In other words, during the PAT selection, as far as possible, Q_{site} must equal Q_{bT}, and H_{site} must equal H_{bT} [12, 26]. The index 0 was added, as in the $n_{sT_{(0)}}$, to represent a preliminary character. Once there is not an infinite number of centrifugal pumps that covers all the scenarios, it is uncertain if there will be a pump whose BEP matches exactly the site parameters.

In order to satisfy this equality, the rotational speed n must be determined. For most cases, when pumps are coupled to 4-pole induction motors, n can be fixed as 1450 rpm. For a given application, statistical analysis on PAT efficiencies relative to the specific speed provide a preliminary way for defining the adequate rotational speed of the motor [12].

The rotation speed n must be chosen so that the specific speed is related to higher

efficiency. This estimation is valid for specific speeds from 5 to 65, with an error of ±5% [12]. Equation 2.8 determines the efficiency curve shown in Figure 2.11. Therefore, from the site parameters, and since higher efficiencies are obtained for specific speed values between 30 and 50, it is possible to estimate the rotational speed by directly substituting these values in Equation 2.7.

$$\eta_{max_T} = -0.00037 n_{sT}^2 + 0.02952 n_{sT} + 0.24326 \tag{2.8}$$

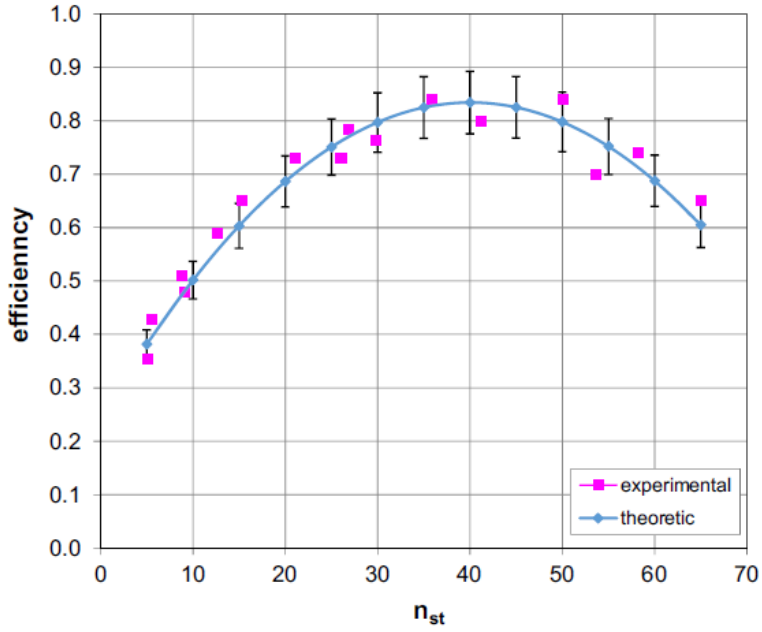

Figure 2.11: Efficiencies at BEP of the PAT sample. Source: Barbarelli et al. [12].

Furthermore, authors linked the specific speed of the pump (n_{sP}) and that of the PAT (n_{sT}), after noticing trends between them throughout the samples, according to Table 2.2. Plus, it is noteworthy that the specific speed of the pump must be greater than that of the turbine.

From the site conditions and hence the desired PAT operating conditions, it is possible to calculate the conversion factors $C_{H_{(0)}}$, $C_{Q_{(0)}}$, and $C_{\eta_{(0)}}$. Based on measures of different samples, authors proposed correlations for these factors through polynomials, covering a wide specific speed range (Table 2.3).

Table 2.2: Correlations between n_{sP} and n_{sT} found in the literature.

Author	n_{sP}
Barbarelli et al. [26]	$0.9867n_{sT} + 5.2818$
Pérez-Sánchez et al. [31]	$1.17619n_{sT}$
Gülich [27]	$\frac{n_{sT}}{0.95\sqrt{\eta_{bP}}}$
Stefanizzi [23]	$\frac{(n_{sT}+2.6588)}{0.9237}$
Yang et al. [41]	$1.125n_{sT} + 1.73$
Fontanella et al. [42]	$\frac{n_{sT}}{0.8793}$

Table 2.3: Correlations for C_H, C_Q, and C_η found in the literature.

Author	C_H	C_Q	C_η
Barbarelli et al. [26]	$-0.000025n_{sP}^3+0.003615n_{sP}^2$ $-0.177396n_{sP}+4.369965$	$0.000221n_{sP}^2$ $-0.022823n_{sP}+1.963005$	–
Pérez-Sánchez et al. [31]	$\frac{1.2337}{n_{sP}}$	$\frac{1}{0.825861\sqrt{n_{sP}}}$	–
Gülich [27]	$\frac{1}{\eta_{bP}^{1.2}}$	$\frac{1}{\eta_{bP}^{0.8}}$	$1.16-\frac{n_{sP}}{200}$
Stepanoff [34]	$\frac{1}{\eta_{bP}}$	$\frac{1}{\sqrt{\eta_{bP}}}$	1
Sharma [35]	$\frac{1}{\eta_{bP}^{1.2}}$	$\frac{1}{\eta_{bP}^{0.8}}$	1
Alatorre-Frenk [36]	$\frac{1}{0.85\eta_{bP}^5+0.385}$	$\frac{0.85\eta_{bP}^5+0.385}{2\eta_{bP}^{9.5}+0.205}$	$1-\frac{0.03}{\eta_{bP}}$
Yang et al. [41]	$\frac{1.2}{\eta_{bP}^{1.1}}$	$\frac{1.2}{\eta_{bP}^{0.55}}$	–

Hence, according to these factors, the required pump parameters $Q_{bP_{(0)}}$ and $H_{bP_{(0)}}$ are obtained and used as input on the manufacturer's chart:

$$Q_{bP_{(0)}} = \frac{Q_{site}}{C_{Q_{(0)}}} \tag{2.9}$$

$$H_{bP_{(0)}} = \frac{H_{site}}{C_{H_{(0)}}} \tag{2.10}$$

Figure 2.12 exemplifies this selection process.

An additional detail to be noticed during the PAT selection is that a minimum back

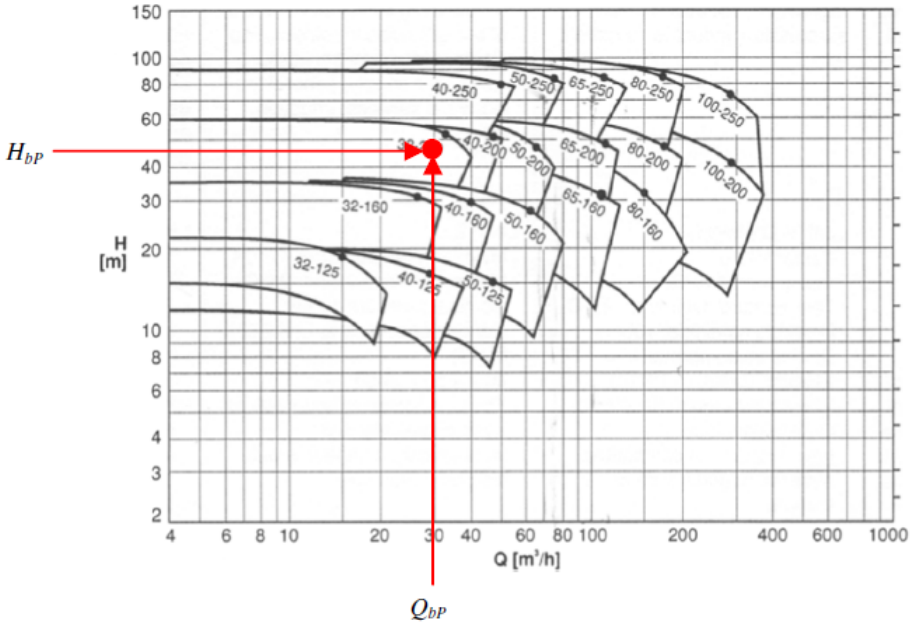

Figure 2.12: First selection of the pump on the manufacturer composite performance chart. Source: Barbarelli et al. [12].

pressure must be available at the outlet nozzle to avoid cavitation problems – noise, vibrations, or material erosion. Such a parameter corresponds to the net positive suction head (NPSH), a measure of the pressure experienced by a fluid on the suction side of a centrifugal pump. It is defined as the total head of fluid at the center line of the impeller less the fluid's vapor pressure. The required NPSH in turbine mode must be 35 to 50% of that in pump operation. An appropriate safety margin recommended is 50% [27].

2.3.2 Performance prediction

Chosen the pump whose parameters match the required ones as closely as possible, it is then known H_{bP}, Q_{bP}, and η_{bP}. Therefore, new values for C_Q, C_H and C_η can be established, as well as the actual specific speed of the pump n_{sP} – by using Equation 2.6 and the ones presented in Table 2.3 again. Thus, reformulating Equations 2.3, 2.4, and 2.5, new relations are obtained to determine H_{bT}, Q_{bT}, and η_{bT}.

$$H_{bT} = C_H \cdot H_{bP} \tag{2.11}$$

$$Q_{bT} = C_Q \cdot Q_{bP} \tag{2.12}$$

$$\eta_{bT} = C_\eta \cdot \eta_{bP} \tag{2.13}$$

The statistical approach of Barbarelli et al. [12] presented the curves that correlates the conversion factors C_H and C_Q to the specific speed of the pump n_{sP} (Figure 2.13). It is worth pointing out that, in order to operate them as turbines and give power, pumps require a minimum flow rate – about 40% of that at BEP considering the sample analyzed.

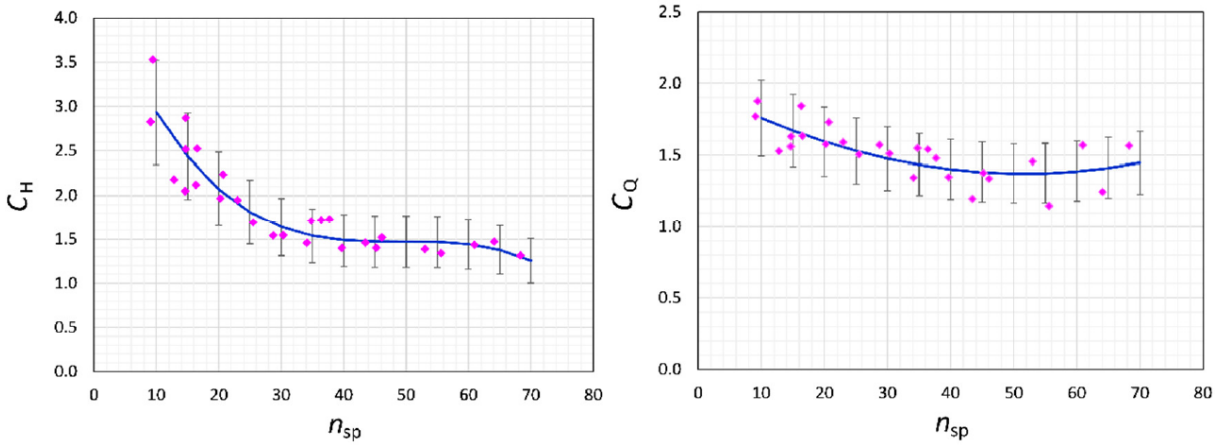

Figure 2.13: Interpolating curves for the conversion factors C_H and C_Q. Source: Barbarelli et al. [26].

Moreover, dimensionless parameters are defined to plot the performance curves, dividing head, flow rate, and power values of the PAT for that at BEP:

$$h = \frac{H_T}{H_{bT}} \tag{2.14}$$

$$q = \frac{Q_T}{Q_{bT}} \tag{2.15}$$

$$p = \frac{P_T}{P_{bT}} \tag{2.16}$$

From experimental data, Barbarelli et al. [12] and Pérez-Sánchez et al. [31] proposed polynomial expressions for h and p as functions of q – the latter also presented the dimensionless efficiency η as a function of q. The former described η as a function of these

parameters and the above-mentioned maximum efficiency of the PAT.

Table 2.4: Expressions for the dimensionless parameters to plot the performance curves.

Author	h	p	η
Barbarelli et al. [26]	$0.922q^2-0.406q$ $+0.483$	$0.040q^3+1.185q^2$ $-0.043q-0.183$	$\frac{p}{hq}$
Pérez-Sánchez et al. [31]	$0.406q^2+0.621q$	$-0.333q^3+2.19q^2$ $-0.863q$	$-1.219q^4+6.95q^3$ $-14.578q^2+13.231q$ -3.383

Figure 2.14 shows dimensionless performance curves for a generic PAT from the sample analyzed by Barbarelli et al. [12]. To get the curves for a real scenario, simply multiply the dimensionless values by the ones at BEP – for each given flow rate value.

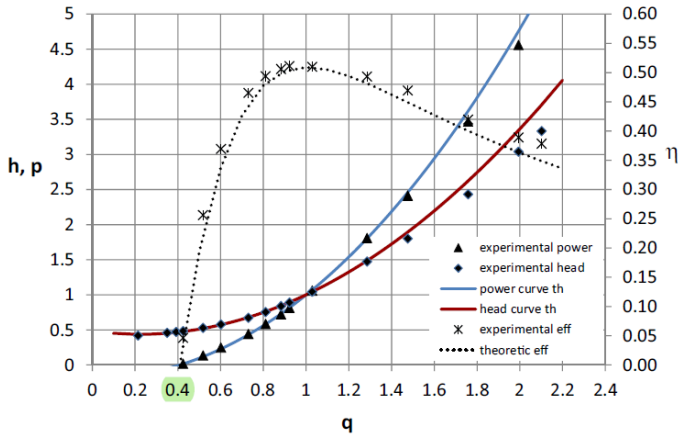

Figure 2.14: Dimensionless curves for a PAT. Source: Barbarelli et al. [12].

As mentioned, the BEP of the pump selected may not exactly coincide with the site parameters. Thus, it is necessary to analyze the operating point and its efficiency. The operating point is the one where the site characteristic curve intersects that of the PAT. Figure 2.16 reports the three possible scenarios for the operating point.

The ideal scenario occurs when the operating point coincides with the BEP (Figure 2.16(a)). The worst scenario occurs when the operating point is on the left of the BEP (Figure 2.16(b)), since in this operating region the efficiency rapidly decreases. When the operating point is on the right of the BEP (Figure 2.16(c)), the efficiency also decreases, but slowly and usually acceptably [12].

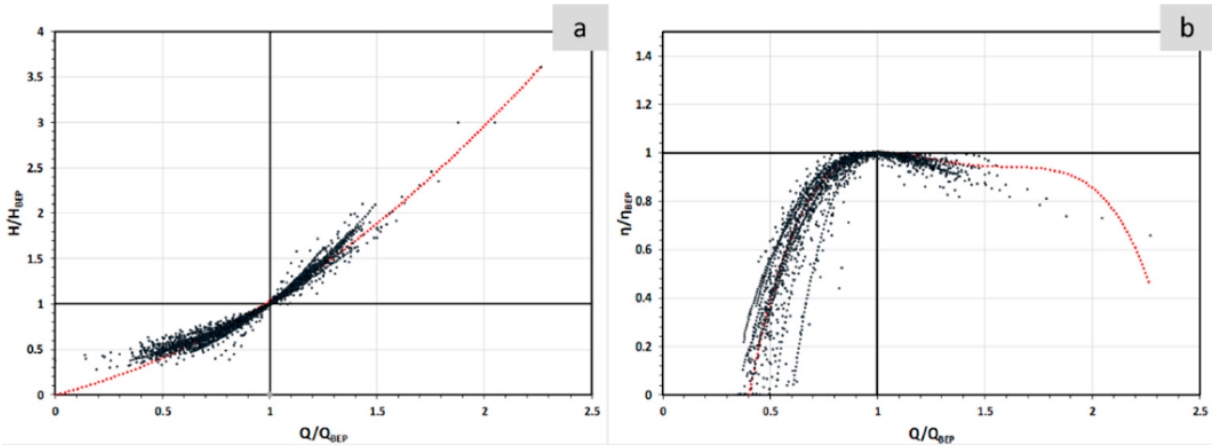

Figure 2.15: Example of $h - q$ (a) and $\eta - q$ (b) predicting curves for a PAT with their sample points. Source: Pérez-Sánchez et al. [31].

Considering operation with invariable rotational speed, it is also recommended the flow rate to be maintained greater than 70% of the BEP in order to avoid a large efficiency drop [31].

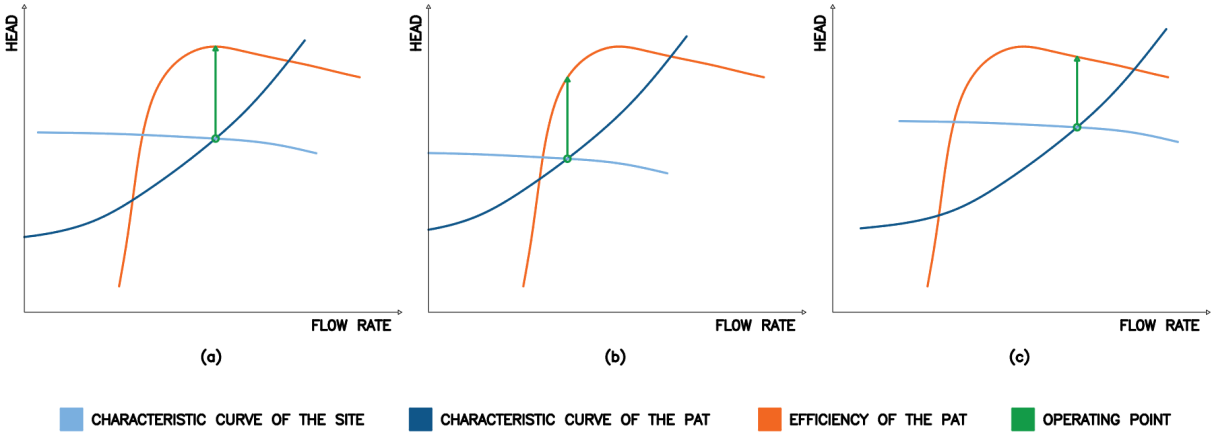

Figure 2.16: Different PAT operating points: (a) ideal, (b) on the left of the BEP, and (c) on the right of the BEP. Adapted from: Barbarelli et al. [12].

Subsequently, runaway $H_L - Q$ and resistance (or zero-speed) $H_W - Q$ curves are important to determine the regulation of the machines, especially the former, as it represents the minimum operation flow of the PAT characteristic curve. Runaway speed refers to an operation with no load – reaching from 120 to 160% of the nominal speed –, achieved either from no-load start-up or load failure, depending on the plant conditions.

Zero-speed refers to a locked rotor condition – the flow rate behavior varies in radial and axial machines [31, 27, 28]. Stefanizzi et al. [23] showed a few scenarios for the PAT operation under different speeds as well as the runaway and the resistance curves (Figure 2.17).

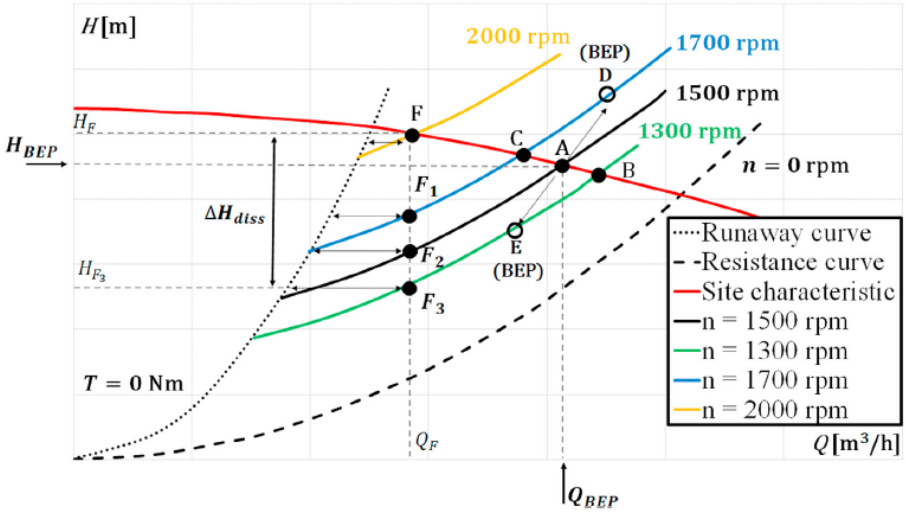

Figure 2.17: PAT characteristic curves at various rotational speeds. Source: Stefanizzi et al. [23].

Gülich [27] defined these curves as parabolas from the origin of the system $H-Q$, since the head is proportional to the square of the flow rate. These curves cannot be predicted from basic principles, so statistical correlations are also used for them. Considering the nominal speed n, the runaway point $(Q_{L,N}, H_{L,N})$ is calculated from the BEP of the turbine. Then, it is possible to obtain the runaway characteristic for any flow rate, as follows [27]:

$$Q_{L,N} = \left(0.3 + \frac{n_{sP}}{400}\right) Q_{bT} \tag{2.17}$$

$$H_{L,N} = (0.55 + 0.002 n_{sP})\, H_{bT} \tag{2.18}$$

$$H_L = H_{L,N} \left(\frac{Q_L}{Q_{L,N}}\right)^2 \tag{2.19}$$

On the other hand, the resistance curve is calculated considering the head as an independent variable, so that the flow rate Q_W for this condition is determined for selected values of head H. Even at locked rotor, a certain flow passes through the turbine which

depends on the flow resistance of the machine [27].

$$Q_W = \left(\frac{41}{n_{sP}}\right)^{0.28} \left(\frac{H}{H_{bP}}\right)^{0.5} Q_{bP} \tag{2.20}$$

If these curves are not too close together, speed control can be applied to the PAT, which is advantageous if the site parameters are close to the BEP. By increasing the rotational speed, the flow rate tends to decrease, and vice versa – obtaining new operating points along the site characteristic curve [23].

In order to implement such speed regulation, a bidirectional frequency converter, or variable frequency drive (VFD), can be connected to the induction machine coupled to the PAT, providing more efficient response to load fluctuation and operational flexibility. However, it results in additional cost and complexity for the system [43].

Basic models and methods to predict the PAT performance have been analyzed so far, which have introduced acceptable calculation errors each other and lead to a global error near to zero. Aidhen et al. [2] made experimental investigations in order to verify and validate different proposed models. For that, a test rig was set up, using a service pump with higher head and flow than those at BEP of the tested pump as a turbine. The tested one was a radial discharge end suction centrifugal pump. Different scenarios were tested by starting the turbine with no load, adjusting the flow rate to reach the desired speed, and then increasing the load by varying the flow at a constant speed.

Studying PAT performance at underrated load and different speeds is essential given the seasonal variation in flow and head available at the site. At considerably high speeds, efficiency may drop marginally. That is why beyond the designed flow, lacking guide vanes for flow control may cause a loss of efficiency since shock losses increase at the entry to the runner and blade tips due to the mismatch between flow direction and vane angle. Moreover, it causes further bearing wear in the coupled induction machine [2, 9].

PAT performance near BEP is smooth, as observed by Aidhen et al. [2], otherwise with efficiency slightly lower than that in pump mode. Within a range of $\pm 20\%$ of BEP flow, a drop in efficiency less than 4% was obtained. It was therefore suggested to operate

a PAT that do not have flow control guide vanes to operate in this range. Away from this, efficiency may considerably decrease. In addition, the best efficiency as a turbine was achieved at higher head and flow compared to pump mode. Gülich [27] attested that a machine achieves essentially the same efficiencies in the turbine and pumping modes, varying in a range of ±2%.

On the other hand, Barbarelli et al. [12], after validating a sample at a test rig, observed that pumps whose specific speed is between 15 and 65 have higher efficiency as a turbine than as a pump. Outside this range, the opposite occurred.

Then, once the PAT is selected and the performance curves are predicted, it is necessary to study the strategies and options for connecting the system to the grid via the coupled generator. The follow section will approach grid connection.

2.4 Grid connection

Regarding the interface between the turbine and the power grid, different types of generators and connection strategies can be applied. Here, an overview of generators and grid connection topologies will be given.

2.4.1 Generators

Considering the range and scope of application of PATs, asynchronous generator (or induction generator) and synchronous generator are worth mentioning below.

Generally, a commercial pump is sold with a three-phase asynchronous motor – typically called an induction motor – as a prime mover, allowing greater cost savings as it is widely available, robust in construction, and has a simple control system [2, 23]. Although more widely used as a motor, an induction machine also can run as a generator. Considering that, a cage induction machine is a viable solution for small electric energy generation units connected to the grid, such as windmills, or with energy recovery systems [13, 44].

Its advantages over synchronous generators include simplicity, price, robustness, and lower maintenance costs. In contrast, almost all large generators in use are synchronous generators [13, 44]. According to the assumptions adopted within the scope of this work, there will be more focus on the induction generator operating with the PAT.

A squirrel-cage rotor induction motor (Figure 2.18) has the same physical stator as a synchronous machine, but a different construction for the rotor – to which there is no direct electrical connection. It is composed of a series of conducting bars placed in slots carved into the rotor face and shorted at both ends by large shorting rings [44].

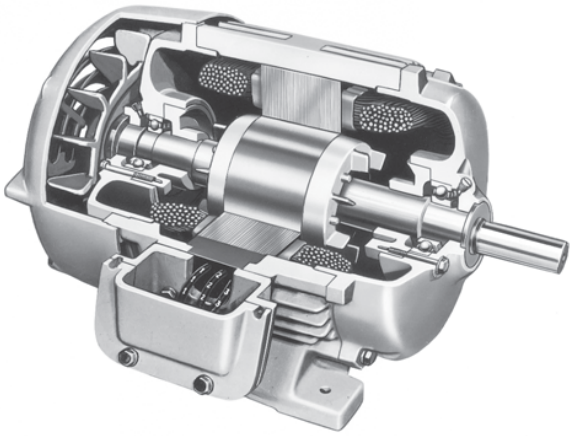

Figure 2.18: Cutaway diagram of a typical small cage rotor induction motor. Source: Chapman [44].

Aidhen et al. [9] describe the electromagnetic process behind the induction machine operating modes:

> "In normal motor operation, the stator flux rotation is faster than the rotor rotation. This causes the stator flux to induce rotor currents, which create a rotor flux with magnetic polarity opposite to stator. In this way, the rotor is dragged along behind stator flux, with the currents in the rotor induced at the slip frequency. In generator operation, a prime mover (turbine or engine) drives the rotor above the synchronous speed (negative slip). The stator flux still induces currents in the rotor, but since the opposing rotor flux is now cutting the stator coils, an active current is produced in stator coils and the

motor now operates as a generator, sending power back to the electrical grid."

Therefore, when connected to a prime mover and rotates above its nominal synchronous speed, the induction "motor" operates as a generator, producing an active current and feeding it back to the power grid – in both grid-connected and standalone systems. Figure 2.19 illustrates the typical torque curve of an induction machine and its operating regions, as well as the PAT torque curve.

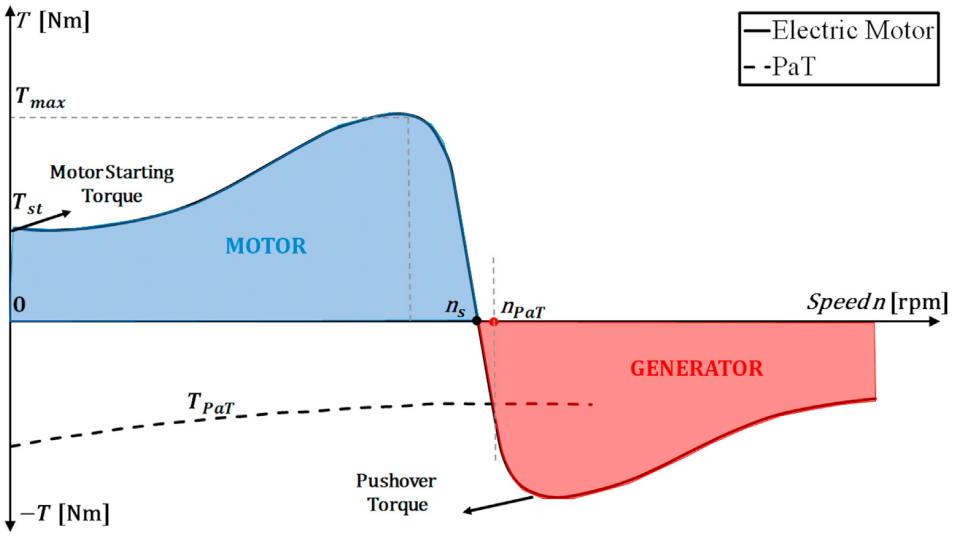

Figure 2.19: Torque curve of an induction machine and PAT torque curve. Source: Stefanizzi et al. [23].

On the other hand, synchronous machines must run at synchronous speed and have their output voltage, which is synchronized with the rotor speed, in phase with the grid – within certain limits. It requires a synchro-check relay and a good turbine speed control. Plus, wound-field synchronous generators also need a separate DC excitation system, with brushes and slip rings, to supply DC voltage to the rotor winding [9, 14]. Several disadvantages are related to this last characteristic, such as regular maintenance and carbon dust cleaning.

In this context, brushless excitation emerges as an alternative. A permanent magnet synchronous generator (PMSG) presents permanent magnets in the rotor to supply the excitation field [44]. Developed for small wind turbines, this solution is typically implemented in low-power and low-cost synchronous generators. The main disadvantage of

these generators is that they have no control of the rotor flux, reaching their peak efficiency only at a preset wind speed. However, recent advances in low speed generators, variable speed systems can be applied beyond conventional structures and will be further explained [7, 15].

In contrast to synchronous generators that require a separate DC excitation system, induction (or asynchronous) generators take reactive power from the grid to provide magnetization current for magnetic field generation. It is also possible for the motor to get its reactive power from a capacitor bank, characterizing a self-excited induction generator (SEIG) – for off-grid applications [2, 13, 9]. Furthermore, the active power generated is proportional to slip above the synchronous speed.

The construction of the induction machine is simpler as it does not require brushes and slip ring arrangement [9]. According to Deprez et al. [13], "for small-scale generation, the induction machine certainly can compete with other generator technologies. However, since the induction machine is mostly used as a motor, the manufacturers' catalogs only mention motor efficiency values". The efficiency curves for these modes are not necessarily the same, depending on the machine's size and efficiency class. The efficiency for generator mode may drop several percent for low power rated and low efficiency machines.

AC generators convert mechanical power into electric power with some loss associated with the process, defining their efficiency. These losses are classified into four basic categories: electrical or copper losses, core losses, mechanical losses, and stray load losses. Copper losses relate to the resistive heating losses in the stator and rotor windings. Core losses occur in the metal of the machine, being the hysteresis and eddy current losses. Mechanical losses are windage and friction losses, associated with mechanical effects. At last, stray (or miscellaneous) losses are further losses that cannot be placed in the previous categories, commonly considered to be 1% of the full load [44].

An indirect method based on the segregation of losses is generally applied to determine the efficiency of an induction machine. Mechanical and core losses are considered constant for both generator and motor modes. Stator copper losses in generator mode are higher than in motor mode once the magnetizing current increases. Rotor losses tend to increase

as the air-gap power increases, but it must take into account the slip factor. The induced voltage is higher in generator mode, and therefore so is the flux, leading to higher magnetic core saturation. Consequently, higher efficiency machines (IE3 and IE4) have comparable efficiencies in both generator and motor operations since they have lower stator and rotor resistances and a non-saturated core [13, 45].

Regarding machine speed control, a synchronous generator demands strict speed control so that its frequency equals line frequency, while an induction generator has a simple control system and is regulated by the power grid. Nonetheless, speed limiting control must be implemented to prevent over speed due to sudden load loss. Plus, a reverse power relay can prevent motorizing in case of speeds below the synchronous one [2].

2.4.2 Grid connection approaches

An induction generator can be easily synchronized to the grid by simply running it up to synchronous speed in the same direction as if the motor were supplied from the grid and connecting to the load [14]. This rotational speed (N_s), depends on the frequency of the system (f) – 50 Hz in Europe –, and the number of magnetic poles of the machine (p_m):

$$N_s\ [rpm] = \frac{120f}{p_m} \tag{2.21}$$

Connecting the generator directly to the grid is possible; however, it may imply large inrush currents and voltage drops. The prime mover speed, for example, affects the amount of transient current and voltage sag during interconnection. Plus, feeder length and load current may affect the voltage drop and compromise the interconnection process – by triggering undervoltage, overcurrent, and circuit breaker to active [14, 46].

For the generator to reach synchronous speed and avoid such undesirable effects, it must be connected through an electronic unit to soft-start the machine or a control valve to mechanically control the turbine shaft power [14]. For remote systems, a SEIG supplying either a three-phase or a single-phase load must be applied [45]. Different ways to connect the generator to the load can be applied whether it is a grid-connected. Once the generator

is connected, for increasing the input power, mechanical power – and therefore rotational speed – from the prime mover also must increase [46]. The release of more flow can be done manually or automatically by means of a valve.

Beyond the direct start, the simpler solution is to connect the generator through an electronic soft-starter, designed to drive three-phase induction machines applied to light duty loads, such as centrifugal pumps, small fans, and screw compressors. A soft starter is designed to protect the machine, allowing for a smooth start and stop, and is an alternative to star-delta and direct on line starting methods. Power thyristors control the applied voltage by adjusting their angle of conduction during starting-up and then are bypassed [47]. A basic implementation circuit using a conventional soft-starter device is proposed in Figure 2.20.

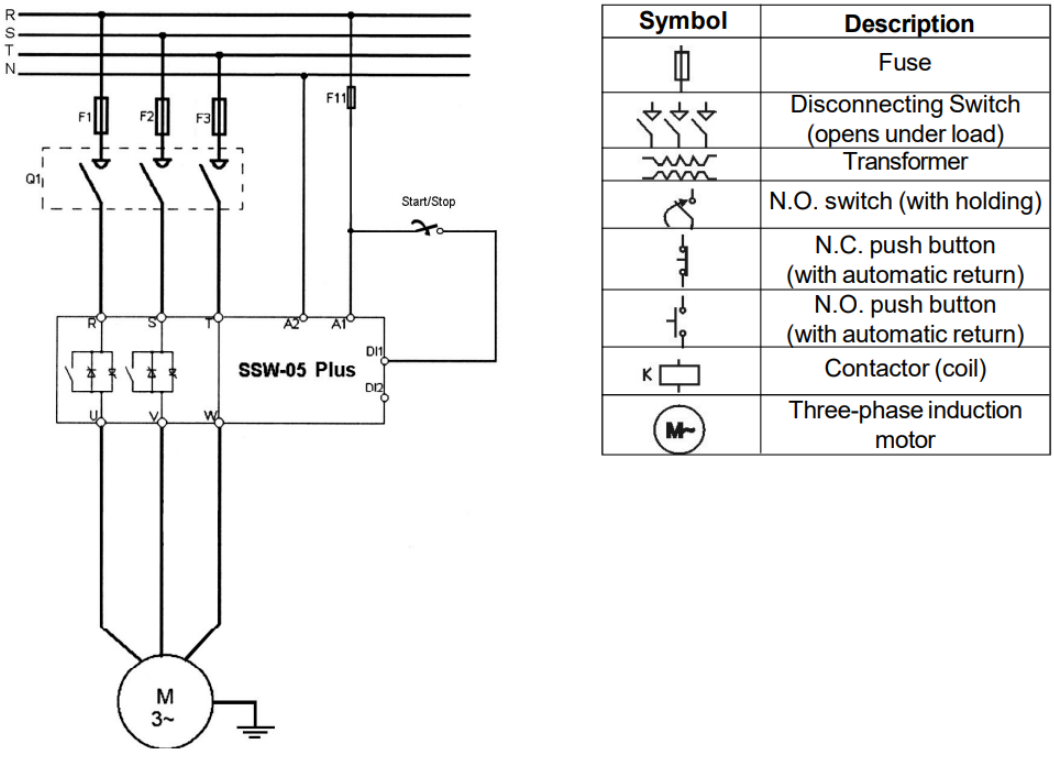

Figure 2.20: Simplified power and control diagram of the soft-starter. Source: WEG [47].

In addition to these grid connection options, inverter-based systems are also a common type of distributed generators – especially in micro-grids. All of these generators

produce alternating current (AC) power, although inverters do not produce it directly, converting direct current power (DC) from devices such as photovoltaic (PV) arrays into AC. Recent approaches with induction or synchronous generators also incorporate PV or wind inverters, hence configuring hybrid systems [48].

As for connection requirements, grid-tie (grid-interactive or synchronous) inverters are the simplest because of their integrated electronics that perform all or most of the protection functions. Some inverters operate only in stand-alone (or off-grid) mode, while others can operate in both modes [48]. Grid-tie inverters are currently off-the-shelf and widely available components used in wind and photovoltaic applications, and a mature and reliable technology in the range of 5 kW [49].

Next, variable and seasonal conditions of head and flow require pico-hydro systems to operate at variable speed, unlike older approaches. Despite their low power, these systems can generate 24 hours a day – in contrast to PV systems that depend on solar irradiation. In this context, further solutions for variable speed pico-hydro systems involving inverter-based systems become viable and attractive, since the inverter compensates for operational fluctuations and interfaces with the grid. Innovative results show that energy generation can be harnessed using inverters in a flexible and efficient way [49, 50].

For such application, instead of a wind inverter with a specific parameterized power curve – as in typical low-power wind systems –, this solution follows a similar idea employing a conventional PV inverter. Pico-hydro turbines behave electrically as PV strings, interacting with conventional PV equipment. Thus, the input voltage of the inverter is the rectified output voltage of the PMSG, which in fact has a different behavior than a PV string. Still, for certain operating conditions and considering the dynamics of the generator, this solution can be reliable and efficient. The implementation and compatibility of standard PV inverters in grid-connected pico-hydro systems were investigated by using a PMSG, a power rectifier bridge, protection circuits, and a PV inverter [20, 15, 50, 51]. Figure 2.21 shows an schematic diagram for this solution.

It is worth pointing out that an over-voltage circuit must be implemented to prevent damage to the generator and inverter in case of no-load conditions. This situation can

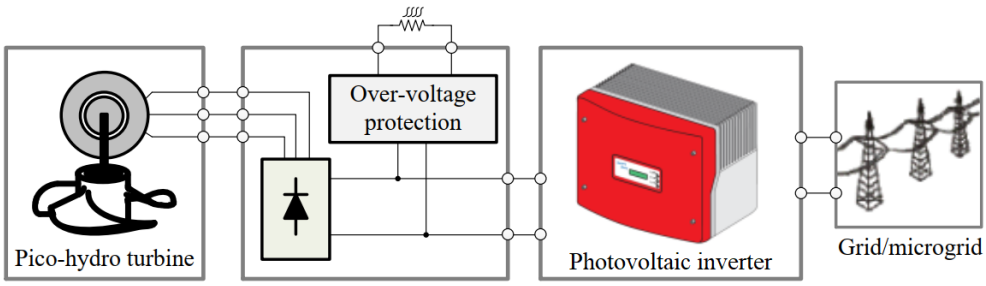

Figure 2.21: Practical approach for grid-connected pico-hydro systems. Source: Leite et al. [20].

occur in case of overpower or whenever the inverter is synchronizing during a grid failure [50]. Recent approaches to simple and low-cost over-voltage protection circuits have been made [51].

Furthermore, recent and modern solutions for grid connection include bidirectional frequency converters, which allow both consuming and injecting power into the grid. Standard VFDs generally aims to run motors at variable speed by applying scalar or vector control and transform one AC component into another with a different frequency by using a pulse-width modulation PWM technique. They are widely available in the market for all power ranges and are reliable, cost-effective, durable, and mass-produced [52].

In short, such devices are composed of a rectifier, a DC-link, and a inverter. The rectifier converts AC voltage to DC voltage. The DC-link stabilizes the DC voltage. The inverter converts the DC voltage back to AC voltage for the AC motor. Some models are also equipped with a brake chopper that connects a external brake resistor to the DC bus voltage when this voltage exceeds its maximum limit – the so-called regenerative braking mode [53]. Manufacturers offer regenerative braking units as optional add-on kits for older versions that do not have them built in. A block diagram is presented in Figure 2.22.

Newer regenerative VFDs capture braking energy from electric motors and return it to the grid, offering a substantial improvement in energy efficiency. The drives can provide significant savings in energy consumption compared to VFDs with the traditional resistor

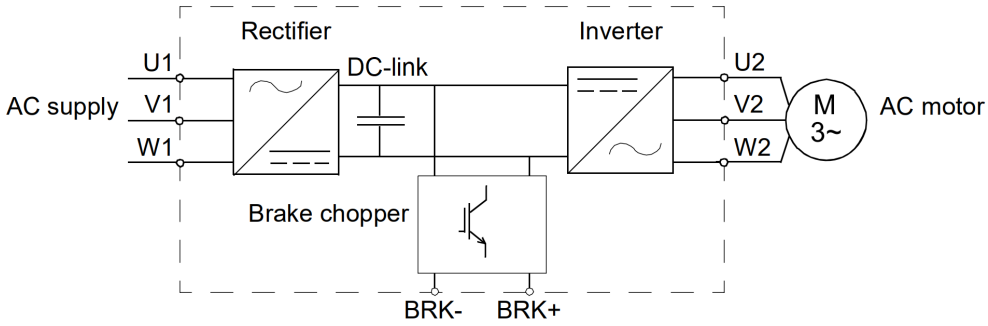

Figure 2.22: Simplified main circuit diagram of a frequency converter. Adapted from: ABB [53].

and mechanical braking methods, where the energy is dissipated as heat and often requires additional cooling. This improvement is feasible by replacing the conventional structure of a rectifier and an inverter with two converters based on insulated gate bipolar transistors (IGBTs) with free wheeling diodes. An additional filter suppresses the harmonics [54].

Thus, the new VFD structure is composed of a LCL filter, a line-side converter, a DC-link, a motor-side converter, and a common mode filter, as shown in Figure 2.23. Hence, the line-side converter can transfer energy from the electrical power grid to the DC-link and vice versa [54].

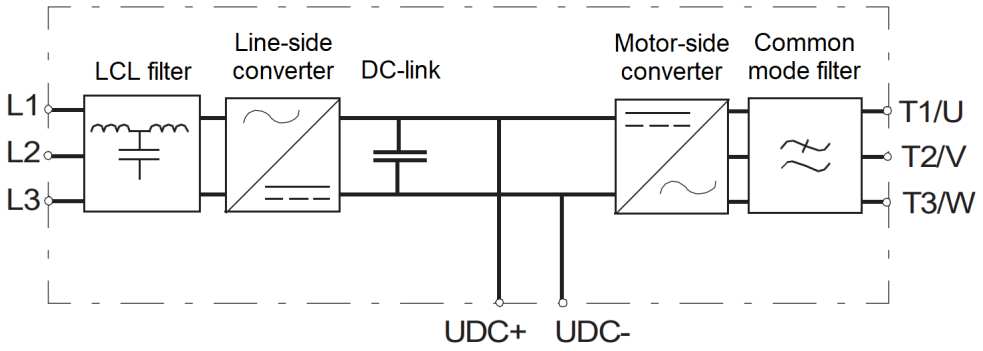

Figure 2.23: Simplified main circuit diagram a regenerative VFD. Adapted from: ABB [54].

Indeed, the application of a regenerative VFD is a very interesting solution for connecting pico-hydro systems to the grid considering its innovative features. For example, it can allow both a soft start of the generator and variable speed control – in additions to

having several built-in protection functions. Notwithstanding, this solution is very recent and still very expensive, which makes its application unfeasible in the scope of this work.

Chapter 3

Site characterization

In this chapter, the context of the implementation of this work is described, highlighting the characteristics of the existing infrastructure, the particularities of the site, and opportunities for improvement, as well as the challenges found. In other words, this chapter aims to approach the context of the Bragança Ciência Viva Centre, where there is hydroelectric potential and where a small hydroelectric system already exists – which faces operation problems.

3.1 Context of the project

The Bragança Ciência Viva Centre (CCVB) is a non-profit scientific and technical association, which belongs to the Portuguese Network of Science Centres of Ciência Viva – constituted by 21 centres present on the continent and on the islands – and is part of the European Network of Science Centres and Museums (ECSITE). Its founding members are the Portuguese Foundation of Science and Technology, the Municipality of Bragança, and the Polytechnic Institute of Bragança (IPB) [49, 16].

Next to the Fervença river, the CCVB is an innovative building, with bioclimatic architecture solutions, allowing to better understand and explore the natural environment through playful experiments – with special emphasis on the younger generation. The CCVB is considered a recognized regional and national reference in terms of its mission

to promote the education of experimental sciences and the communication of science and culture [55]. Figures 3.1 and 3.2 show the CCVB facilities and the surroundings of the site.

Figure 3.1: The CCVB on the bank of the Fervença River.

The headquarters of the CCVB is located where, at the beginning of the 20^{th} century, a hydroelectric power plant was installed on the left bank of the Fervença River, which used the energy of the river waters to generate power for the city until the 1960s. In the 2000s, the riverside area upstream of the Silk House, which is part of the CCVB and is next to the downstream dam, was re-qualified. Several small dams were built in order to create "water mirrors".

The CCVB is a smart and eco-efficient building and currently has a micro-power plant consisting of a forced duct and a hydroelectric plant, with a 15 kW low-voltage generator set [16, 17]. The micro-hydro plant was licensed as a micro-generation unit years ago, injecting all the energy generated into the grid. However, the current sale price no longer makes its operation rentable. Figure 3.3 shows the existing generator and its infrastructure.

Figure 3.2: Satellite view of the CCVB. Adapted from: Google Maps [56].

Figure 3.3: 15 kW hydroelectric generator in the CCVB.

Unfortunately, this system has recently experienced some difficulties in its operation. The system demands too much flow from the river – around 600 m^3/h – considering the current rainfall index and the climatic differences throughout the year, substantially interfering with the volume of water in the dams. The penstock and the system were sized for a flow that is currently impractical in the context of the river.

The existing infrastructure, which operates for a short time per year, would be better utilized on a self-consumption basis for the building. Still, the nominal power of the system is greater than the actual need of generation for self-consumption in the plant during most of the year. Since the system has a conventional hydraulic turbine, skilled labor is not widely available for maintenance, nor are spare parts for replacement.

Consequently, considering the characteristics and the advantages of the application of PATs in the context of small-scale hydropower plants, there is an opportunity to study the implementation of such an approach in the context of the CCVB, taking advantage of the existing hydroelectric potential and being an alternative to the existing infrastructure – which although it has already been repaired, it will continue to operate for a short period of the year. An alternative is a generation organized in power levels, which is more profitable in the context of self-consumption. Even at lower power, a perennial operation results in considerable power generation.

3.2 Consumption data and site parameters

First, energy consumption data was collected using recent energy bills and load diagrams of the CCVB facilities. Energy bills for all months of 2021 were made available for study, as well as load diagrams for seven months of 2021 and three months of 2022. An example of the energy bill is shown in Figure 3.4, for December 2021, which will later be considered in the consumption survey.

The centre is open from 10 a.m. to 6 p.m. Tuesday through Friday and 11 a.m. to 7 p.m. on Saturdays and Sundays, remaining closed on Mondays. Sometimes, especially on Fridays, some activities last up to 24 hours. The site's electricity supply is of the special

NIPC:
Nome do Cliente: Centro Ciencia Viva De Bragança

Morada Local Consumo: Centro De Ciência Viva Centro De Ciência Viva Centro De Ciência Viva, ., Bragança, 5300-263 Bragança

Código Ponto Entrega:
Tarifa: Tetra **Nível Tensão:** BTE **Ciclo Horário:** Ciclo Diário

DETALHES DA FATURA

Eletricidade

	Período a Faturar		Quantidades	Preço Unit.	Nº Dias	% IVA	Valorização
	Data início	Data fim	(kWh/kVArh/kW)				(s/IVA)
Energia Ativa							€
Super Vazio (SV)	02/12/2021	01/01/2022	1.312,0000	€		23%	€
Vazio Normal (VN)	02/12/2021	01/01/2022	1.958,0000	€		23%	€
Ponta (P)	02/12/2021	01/01/2022	1.364,0000	€		23%	€
Cheia (C)	02/12/2021	01/01/2022	4.048,0000	€		23%	€
Redes							€
Redes Super Vazio (SV)	02/12/2021	31/12/2021	1.269,6774	€		23%	€
Redes Super Vazio (SV)	01/01/2022	01/01/2022	42,3226	€		23%	€
Redes Vazio Normal (VN)	02/12/2021	31/12/2021	1.894,8387	€		23%	€
Redes Vazio Normal (VN)	01/01/2022	01/01/2022	63,1613	€		23%	€
Redes Ponta (P)	02/12/2021	31/12/2021	1.320,0000	€		23%	€
Redes Ponta (P)	01/01/2022	01/01/2022	44,0000	€		23%	€
Redes Cheia (C)	02/12/2021	31/12/2021	3.917,4194	€		23%	€
Redes Cheia (C)	01/01/2022	01/01/2022	130,5806	€		23%	€
Potência Contratada	02/12/2021	31/12/2021	41,4100	€	30	23%	€
Potência Contratada	01/01/2022	01/01/2022	41,4100	€	1	23%	€
Potência Horas de Ponta	02/12/2021	31/12/2021	11,0000	€	30	23%	€
Potência Horas de Ponta	01/01/2022	01/01/2022	11,0000	€	1	23%	€
Escalão 1 de En.React.cons.FV	02/12/2021	31/12/2021	523,7400	€		23%	€
Escalão 2 de En.React.cons.FV	02/12/2021	31/12/2021	523,7400	€		23%	€
Escalão 3 de En.React.cons.FV	02/12/2021	31/12/2021	648,3900	€		23%	€
Escalão 1 de En.React.cons.FV	01/01/2022	01/01/2022	17,4600	€		23%	€
Escalão 2 de En.React.cons.FV	01/01/2022	01/01/2022	17,4600	€		23%	€
Escalão 3 de En.React.cons.FV	01/01/2022	01/01/2022	21,6100	€		23%	€

Figure 3.4: Composition of a CCVB energy bill.

low voltage (BTE - *Baixa Tensão Especial*) and three-phase system, with a contracted power of 41.41 kVA, presenting a four-hourly tariff with a daily cycle. In this case, the hours of the day are divided among four categories with different billing values, whose configuration also varies if they are months with summer or winter legal time. Figure 3.5 shows how the schedule is classified.

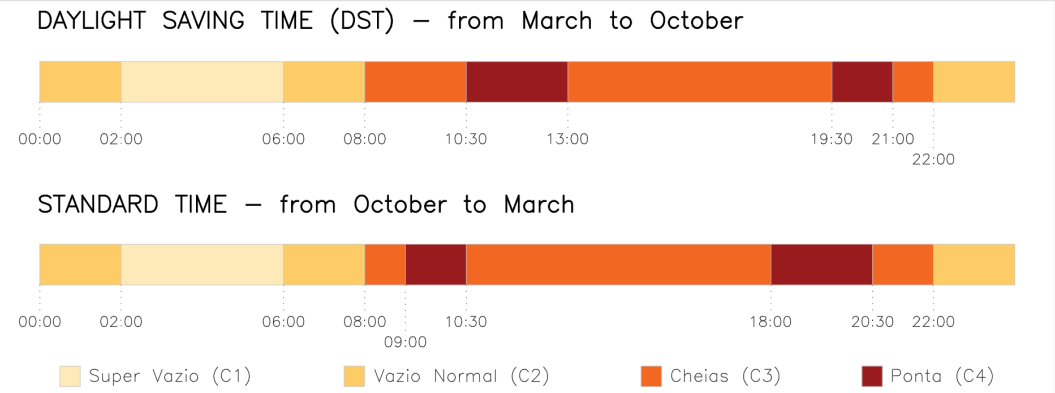

Figure 3.5: Daily cycle for BTE consumers. Adapted from: EDP [57].

From the energy bills, a survey was made of the energy consumption billed in categories C1, C2, C3, and C4, as shown in Figure 3.6. It can be seen that consumption is higher during the winter period when more flow is available in the river. Consumption in the summer months, at a lower level, is also considerable; however, the lack of rain at that time can determine the reduced or inactive operation of the hydroelectric system. The consumption trend in the spring and fall months is similar – except for November and early December when there is already a transition to the colder season.

Considering the sum of all categories, the total consumption during 2021 was approximately 52,500 kWh. Thus, the monthly average of this consumption was about 4,375 kWh, with a maximum average value of about 8,000 kWh during the three coldest months and a minimum of 2,430 kWh during the milder weather months. The average daily consumption that year was approximately 144 kWh. Moreover, excess reactive power consumption was found in several energy bills, which – outside the scope of this work – indicates the need to implement a capacitor bank for reactive power compensation. In fact, assuming a self-consumption scenario, less active power from the grid will be required, which further

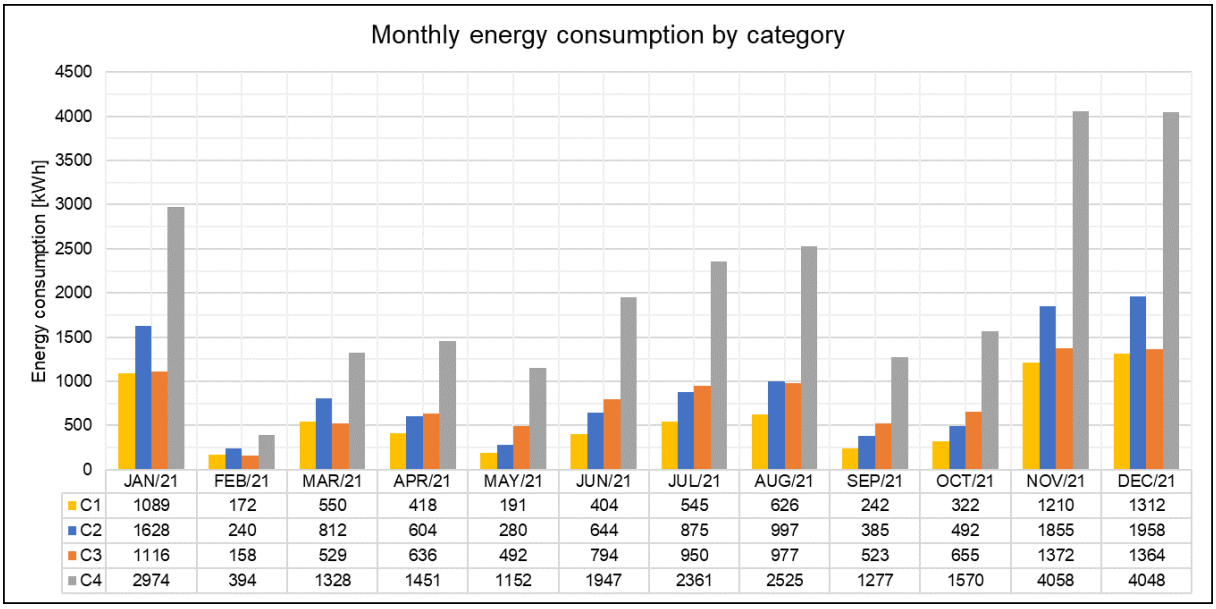

	JAN/21	FEB/21	MAR/21	APR/21	MAY/21	JUN/21	JUL/21	AUG/21	SEP/21	OCT/21	NOV/21	DEC/21
C1	1089	172	550	418	191	404	545	626	242	322	1210	1312
C2	1628	240	812	604	280	644	875	997	385	492	1855	1958
C3	1116	158	529	636	492	794	950	977	523	655	1372	1364
C4	2974	394	1328	1451	1152	1947	2361	2525	1277	1570	4058	4048

Figure 3.6: CCVB's monthly energy consumption divided into categories.

impacts the installation's power factor.

For a better reading of the consumption demanded, an analysis of the facility's load diagrams was also made available for the 12 different months of the year – from January to March 2022 and from April to December 2021. The data was processed, and an average scenario was put together for a typical workday for each station analyzed, as shown in the graph in Figure 3.7.

The curves of power consumed by the facility are coherent concerning the operating hours of the CCVB, increasing demand between 10 and 11 a.m. and gradually decreasing from 6 p.m. One can observe that there is a minimum power consumed during the days, practically constant during the hours when the centre is closed, but which changes proportionately according to the time of year. The average power consumed between 7 p.m. and 10 a.m. was 10.9 kW in the winter and 2.9 kW in the spring. Nevertheless, it was observed that between September 9^{th} 2021 and October 25^{th}, a period corresponding to approximately half a season (47 days), the demanded power curve reached its minimum level during non-working hours. The average value in this period was 1.7 kW.

It is worth mentioning that there was also a significant increase in consumption from

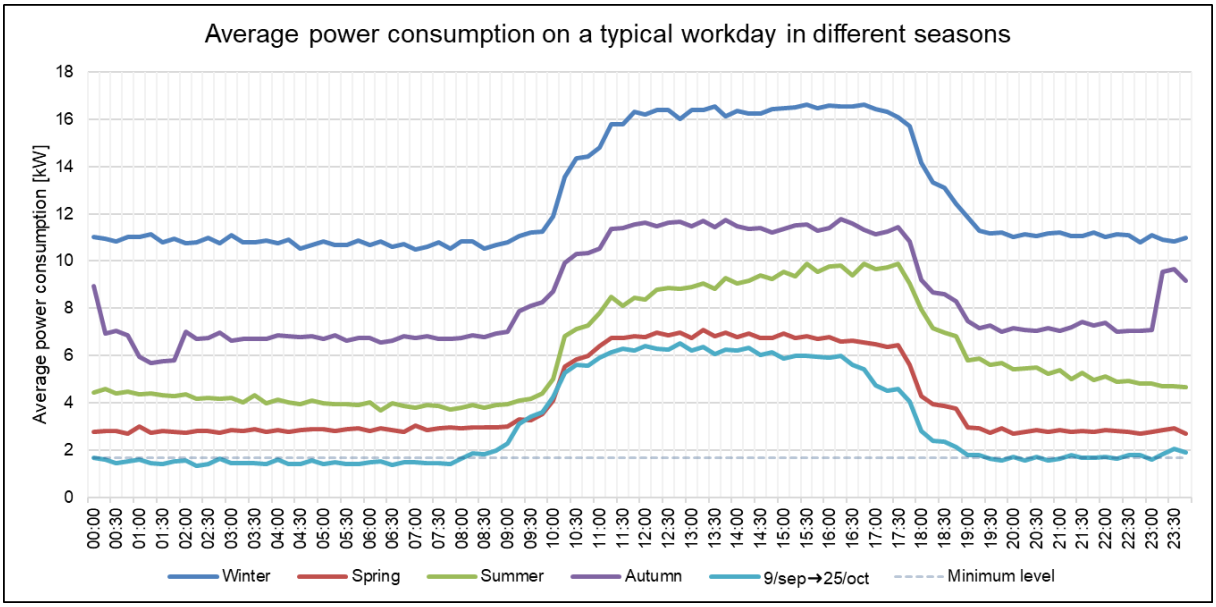

Figure 3.7: Average energy consumption of the CCVB on a typical workday in different seasons.

January to March, comparing the years 2021 and 2022. The return of activities post-pandemics justifies this scenario, considering that the CCVB remained closed to the public from January 17 to April 5, 2021.

Based on the 12 months measured (275 days of 2021 and 90 days of 2022), total consumption of approximately 64,416 kWh was found during this one-year period, with an average daily consumption of 176 kWh. This consumption growth resulted from January, February, and March data, since the operation was not interrupted during the beginning of that year – as it had been in the previous one. In these months, the increase in consumption was 108%. The expectation is that with the resumption of full operation of services after the pandemic period, consumption in the following months of the year will also be higher – even if not as significantly, since there will be no total interruption of services as of April 2021.

The site where the CCVB is located has an attractive hydroelectric potential, considering its proximity to the Fervença river bank and the existing topography. The head available at the site is 13 m, with slight fluctuation throughout the year. However, based on site knowledge and previous studies [58], one must first consider that the period of

operation of a hydropower system at this site must not exceed 7 to 8 months due to dry summer months when the flow is significantly reduced. In the scope of this work, the available flow will be considered at around half of the flow demanded by the existing generator, which represents around 600 m^3/h, so as not to cause significant impacts on the river's natural flow.

Chapter 4

Application and Results

In the context of the CCVB, alternatives developed to adequately exploit the existing potential from small-scale hydropower systems are presented using PATs. The PAT selecting procedure is applied for this context, composing the technical solution developed. Moreover, it includes a discussion about the results obtained from this work and additional tests for new approaches.

4.1 Application of the State of the Art

4.1.1 Initial considerations

A new hydropower system can be implemented to replace or complement the current one, taking advantage of the existing structure and adapting to the new characteristics. The design of a pico-hydro system using PATs requires the selection of one or more pumps appropriate to the information and conditions available at the site, which was described generically in Section 2.3.

PATs will be implemented for the CCVB context since their functioning is more suitable to the environment and the available conditions than the existing system. Plus, they can constitute a perennial solution of low cost and with equipment widely available on the market – besides having more straightforward and easily accessible maintenance. A

basic scheme of the project is presented in Figure 4.1.

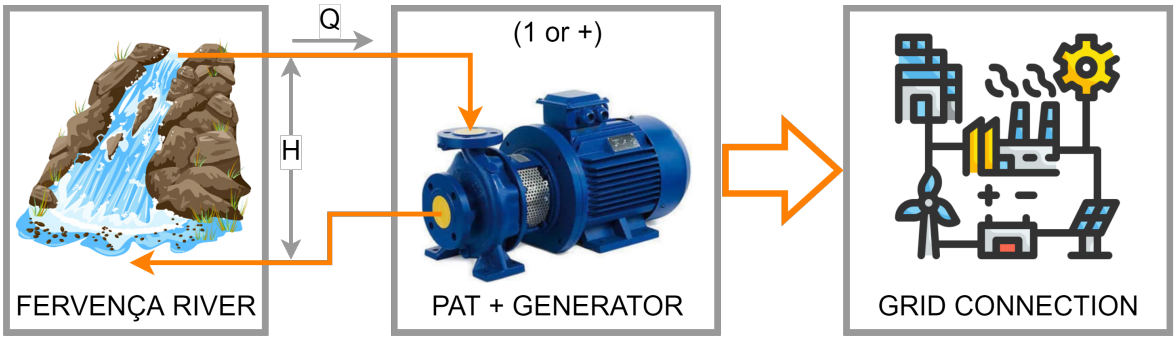

Figure 4.1: Basic scheme of the project.

Installing a system that works in power levels – requiring more flow during the wetter seasons and less during the drier ones – is an interesting solution, considering the variable availability of head and especially flow. If a bidirectional VFD were used, a unique pump could be implemented to operate at different power levels. However, the price of this device is equal to or even higher than that of the pump. Plus, it has more complex installation, commissioning, and maintenance, which are difficult to obtain from local companies. Thus, in this scope of this work, more than one PAT is implemented to obtain different power levels.

Firstly, head and flow rate values are preliminarily considered to draft the system. Considering that the existing piping will add a head loss of less than 10% as it was sized for a much greater flow, a head of 12 m is assumed to be usable for the system. Also, a maximum flow rate of 300 m^3/h, half of the flow demanded by the existing generator, is considered. Using Equation 2.2, it is possible to quickly estimate the generated electrical power of a small-scale hydropower system using a PAT, potentially obtained from these parameters:

$$\begin{aligned} P_o = \eta_g \cdot P_h = 0.85 \left(0.78 \times 9.81 \times 12 \times \frac{300}{3600}\right) \\ P_o = 0.85 \times 7.65 = 6.5\ [kW] \end{aligned} \tag{4.1}$$

Therefore, a hydraulic power of 7.65 kW and a generated electrical power of 6.5 kW

were obtained preliminarily. From these power references and consumption data, one can stipulate power level values employing two PATs, as follows:

- Level 1: A smaller PAT to mainly supply low consumption during non-working hours;
- Level 2: A second PAT, greater than the first, to supply the consumption or as a supplement during office hours;
- Level 3: Both PATs supply a higher consumption during office hours.

These two combined must have hydraulic power less than or equal to that calculated above for the maximum flow rate. This range does not significantly impact the river during most of the year. Given the available head, it already represents a valuable power in the context of the science living center. Moreover, considering the configuration of distributed generation systems for self-consumption, a system with generation power closer to the consumption of the facility's loads is preferable.

In this regard, two different pumps will be studied as PATs, each in a different situation, meeting the requirements of the power levels and corresponding to the instant energy demand. According to the collected consumption data, it is possible to note a minimum demanded power level throughout the year, during non-working hours between 9^{th} 2021 and October 25^{th}, which is approximately constant at around 1.7 kW. During the day, the consumption varies among different seasons, reaching peaks of 7.1 kW in the spring and 16.6 kW in the winter – on typical days for each.

The first PAT must be selected to supply electrical power close to this minimum value. In order to supply greater power during office hours, a pump available in the IPB lab, previously used in testing for other hydraulic systems, will be analyzed for implementation as the second PAT.

4.1.2 Selection and performance prediction of the PATs

The procedure for selecting the PATs and predicting their performance is explained in more detail for the first one, according to the flow chart in Figure 2.9. For the second PAT, the procedure does not include the pump selection, as the existing one in the laboratory will be tested. From this part on, the procedure is quite similar and therefore summarized.

For selecting the first PAT, the flow rate, given the available head, is estimated to provide the necessary electrical power using Equation 2.2 again:

$$\begin{aligned} P_o = 1.7\,[kW] \Rightarrow 0.85\,(0.78 \times 9.81 \times 12 \times Q) = 1.7 \\ Q = \frac{1.7}{78.05} = 0.022\,[m^3/s] \end{aligned} \tag{4.2}$$

In addition, one must determine the rotational speed of the pumps running as turbines to be selected. Then, a preliminary specific speed related to higher efficiency is adopted for the site – according to Figure 2.11 and Equation 2.7. From a preliminary specific speed $n_{site_{(0)}}$ of 40, the rotational speed $n_{(0)}$ obtained is:

$$\begin{aligned} n_{site_{(0)}} = 40 \Rightarrow \frac{n_{(0)}\,0.022^{0.5}}{12^{0.75}} = 40 \\ n_{(0)} = \frac{40}{0.023} = 1747\,[rpm] \end{aligned} \tag{4.3}$$

Pumps are generally sold coupled to 2, 4, and 6-pole induction motors, corresponding to rotational speeds of approximately 960, 1450, and 2900 rpm – respectively [59]. Therefore, the commercial value adopted for the rotational speed is 1450 rpm since it is the closest available. From this new reference and the equation just used, the actual specific speed related to the site n_{site} is calculated to be 33.19, which must match the specific speed of the later chosen PAT ($n_{sT_{(0)}}$).

Established the site parameters H_{site}, Q_{site}, and n_{site}, the specific speed of the pump ($n_{sP_{(0)}}$) linked to that of the PAT is then obtained using the correlations in Table 2.2. Also, a preliminary approach uses a turbine efficiency of 78% [9]. Table 4.1 presents the values obtained for n_{sP} according to different authors. It is important to emphasize

that the mean values obtained from the correlations proposed by different authors are considered in this process.

Table 4.1: Results obtained for $n_{sP_{(0)}}$.

Author	$n_{sP_{(0)}}$
Barbarelli et al. [26]	38.03
Pérez-Sánchez et al. [31]	39.04
Gülich [27]	39.56
Stefanizzi [23]	38.81
Yang et al. [41]	39.07
Fontanella et al. [42]	37.75
MEAN	38.71

Next, it is possible to determine the conversion factors $C_{H_{(0)}}$, $C_{Q_{(0)}}$, and $C_{\eta_{(0)}}$ from Table 2.3.

Table 4.2: Results obtained for $C_{H_{(0)}}$, $C_{Q_{(0)}}$, and $C_{\eta_{(0)}}$.

Author	$C_{H_{(0)}}$	$C_{Q_{(0)}}$	$C_{\eta_{(0)}}$
Barbarelli et al. [26]	1.470	1.411	–
Pérez-Sánchez et al. [31]	1.582	1.371	–
Gülich [27]	1.347	1.220	0.966
Stepanoff [34]	1.282	1.132	1.000
Sharma [35]	1.347	1.220	1.000
Alatorre-Frenk [36]	1.586	1.601	0.962
Yang et al. [41]	1.577	1.376	–
MEAN	1.456	1.333	0.982

At that point, $C_{\eta_{(0)}}$ is not yet used. From the factors $C_{Q_{(0)}}$ and $C_{H_{(0)}}$, $Q_{bP_{(0)}}$ and $H_{bP_{(0)}}$ are obtained according to Equations 2.9 and 2.10.

$$Q_{bP_{(0)}}\,[m^3/h] = \frac{0.022 \times [3600]}{1.333} = 58.83\,[m^3/h] \tag{4.4}$$

$$H_{bP_{(0)}} = \frac{12}{1.456} = 8.24\,[m] \tag{4.5}$$

Then, these values are input into the manufacturer's chart to choose a suitable pump, as presented in Figure 4.2.

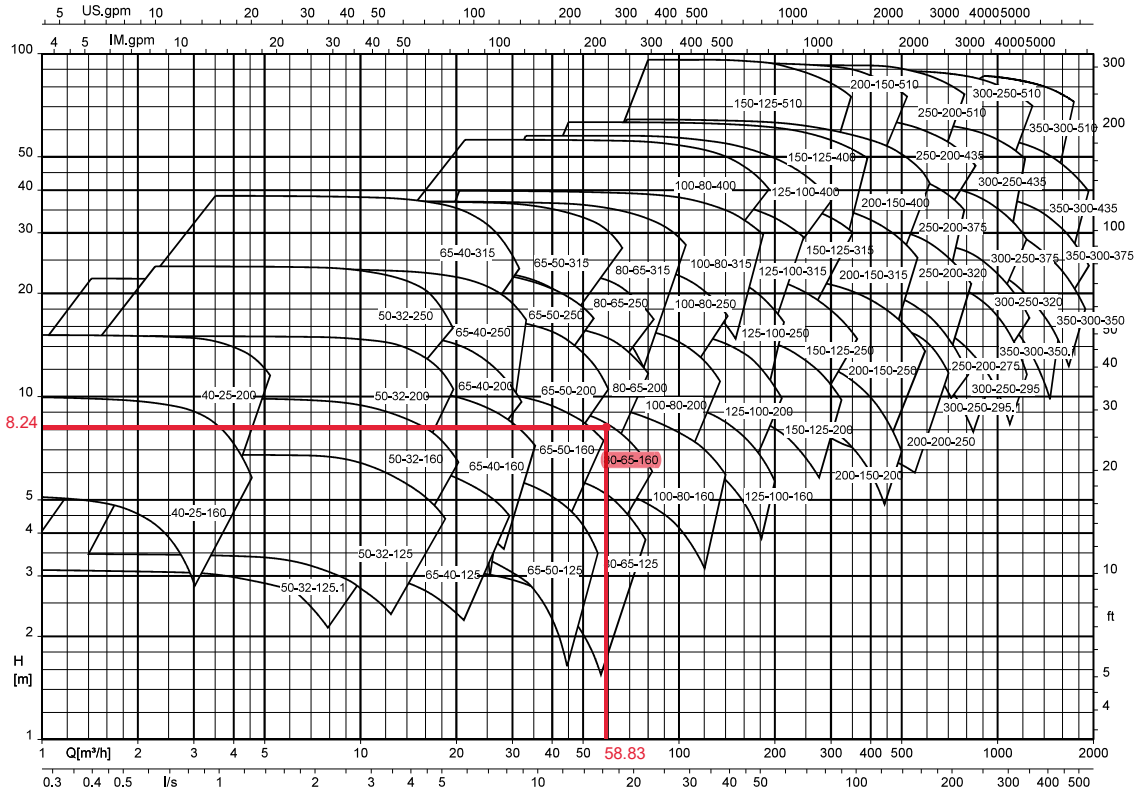

Figure 4.2: Pump selection from manufacturer's chart. Source: KSB [59].

After choosing the pump – in this case, the model KSB 080-065-160 present in the manufacturer's chart –, values for H_{bP}, Q_{bP}, and η_{bP} are obtained from the characteristic curves in the catalog. From Figure 4.3, it is concluded that: $H_{bP} = 8.50$ m; $Q_{bP} = 57.60$ m^3/h; and $\eta_{bP} = 81.8\%$. The impeller diameter adopted is 174 mm, better fitting the head and flow rate values.

Then, new values for n_{sP}, C_Q, C_H, and C_η are established using Equation 2.6 and Table 2.3 again, as follows:

$$n_{sP} = \frac{1450\,(57.6/3600)^{0.5}}{8.50^{0.75}} = 36.84 \tag{4.6}$$

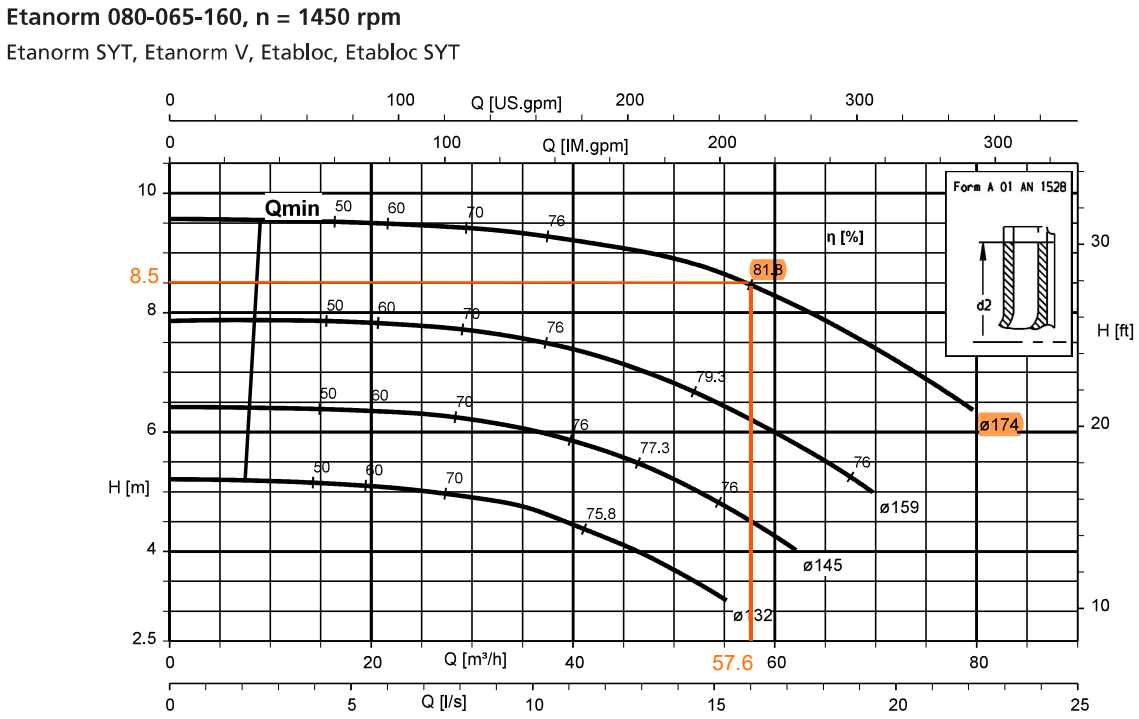

Figure 4.3: Characteristic curves of the pump 080-065-160. Source: KSB [59].

Later on, from Equations 2.11, 2.12, and 2.13, the PAT parameters – H_{bT}, Q_{bT}, and η_{bT} – are determined at BEP. These represent the best-operating conditions for the selected pump to run as a turbine, which are different from the regular operation and not necessarily those available at the site studied.

$$\begin{aligned} H_{bT} &= 1.386 \times 8.50 = 11.78\ [m] \\ Q_{bT} &= 1.278 \times 57.60 = 73.59\ [m^3/h] \\ \eta_{bT} &= 0.985 \times 81.8\% = 80.6\% \end{aligned} \tag{4.7}$$

In order to know the operating conditions at the site, it is necessary to plot and analyze the PAT performance curves. The dimensionless parameters from Table 2.4 are used to plot these curves. Arbitrary values must be assigned for the parameter q to obtain the other parameters for each scenario. On this basis, values for q are varied from zero to a value corresponding to twice that at BEP – in a step such that the plotted curves

Table 4.3: Results obtained for C_H, C_Q, and C_η for the first PAT.

Author	C_H	C_Q	C_η
Barbarelli et al. [26]	1.491	1.422	–
Pérez-Sánchez et al. [31]	1.508	1.339	–
Gülich [27]	1.273	1.174	0.976
Stepanoff [34]	1.222	1.106	1.000
Sharma [35]	1.273	1.174	1.000
Alatorre-Frenk [36]	1.436	1.388	0.963
Yang et al. [41]	1.497	1.340	–
MEAN	1.386	1.278	0.985

are reasonably smooth. Additionally, the runaway curve is also traced to represent the minimum operation flow of the PAT characteristic curve (Equations 2.17, 2.18, and 2.19).

Figure 4.4 shows the performance curves obtained using the methods proposed by (a) Pérez-Sánchez et al. [31] and (b) Barbarelli et al. [12].

From the performance information and considering the available head of 12 m, the operational values for the flow rate and efficiency of the PAT – hereinafter called PAT 080-065-160 – can be determined, which are shown in Table 4.4.

Table 4.4: Operating values for PAT 080-065-160.

Method	$Q_T\ [m^3/h]$	$P_T\ [kW]$	$\eta_T\ [\%]$
Barbarelli et al. [26]	74.59	1.96	80.5
Pérez-Sánchez et al. [31]	73.17	1.86	80.6
MEAN	73.88	1.91	80.6

Finally, from a hydraulic power of 1.91 kW and a generator efficiency of 85% [30], the generated electrical power will equal 1.63 kW – close to the minimum demanded power of 1.7 kW. Hence, one concludes that the selected pump can meet the requirements and be applied in Level 1 to supply low consumption during non-working hours. Moreover, as long as it is during months of operation, this power level can operate 24 hours a day,

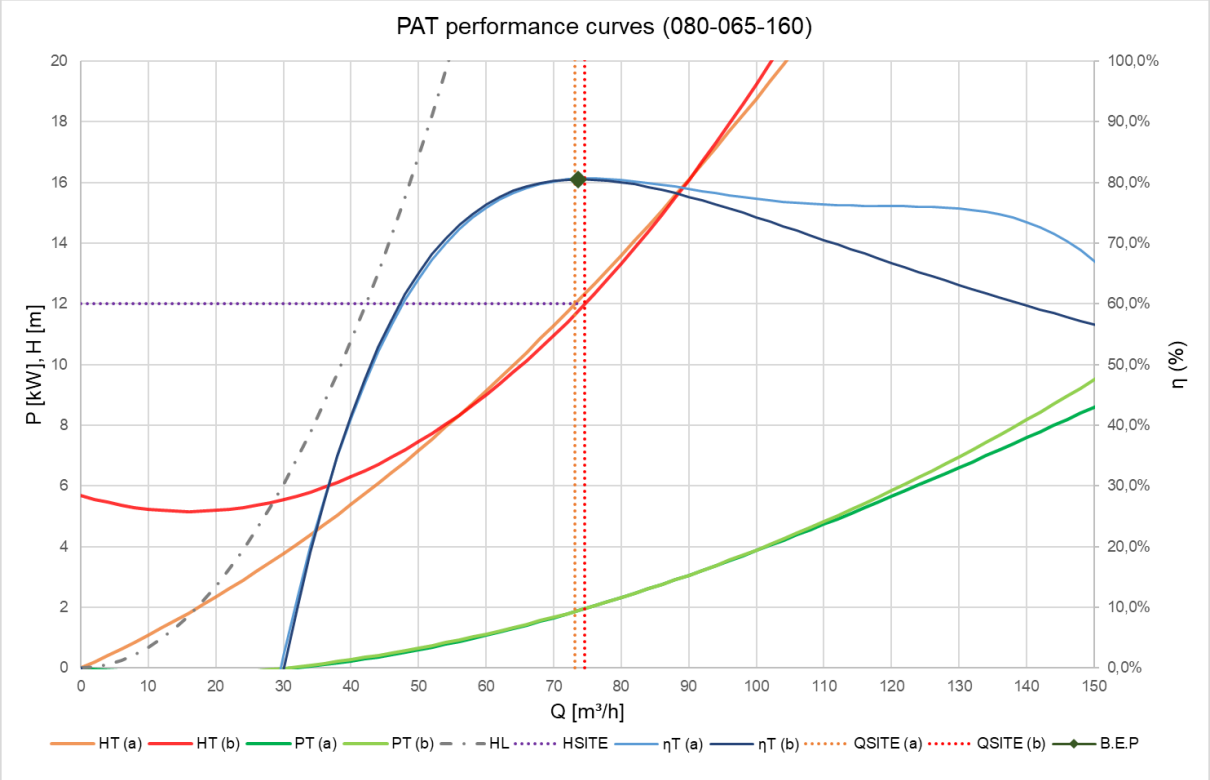

Figure 4.4: PAT performance curves for the pump 080-065-160.

as this energy will be consumed in the building even during the minimum consumption times.

Afterwards, the performance prediction procedure is repeated for the second PAT considering the 5.5 kW pump available in the lab (Figure 4.5): model Wilo CronoBloc-BL-E 125/185-5,5/4; coupled to a 4-pole induction motor (η >85%); n = 1450 rpm; impeller diameter of 189 mm. The main characteristics are similar to that of the first pump, however, for greater power. Thus, characteristic curves are presented in Figure 4.6.

Figure 4.5: CronoBloc-BL-E 125/185-5,5/4.

From Figure 4.6: H_{bP} = 8.40 m; Q_{bP} = 192 m^3/h; and η_{bP} = 83%.

- Results for n_{sP}, C_Q, C_H, and C_η are presented in Equation 4.8 and Table 4.5;
- Results for H_{bT}, Q_{bT}, and η_{bT} are presented in Equation 4.9;
- Performance curves are traced in 4.7 using the methods proposed by (a) Pérez-Sánchez et al. [31] and (b) Barbarelli et al. [12].
- Operational values obtained from performance information and available head are presented in Table 4.6.

$$n_{sP} = \frac{1450\ (192/3600)^{0.5}}{8.40^{0.75}} = 67.87 \tag{4.8}$$

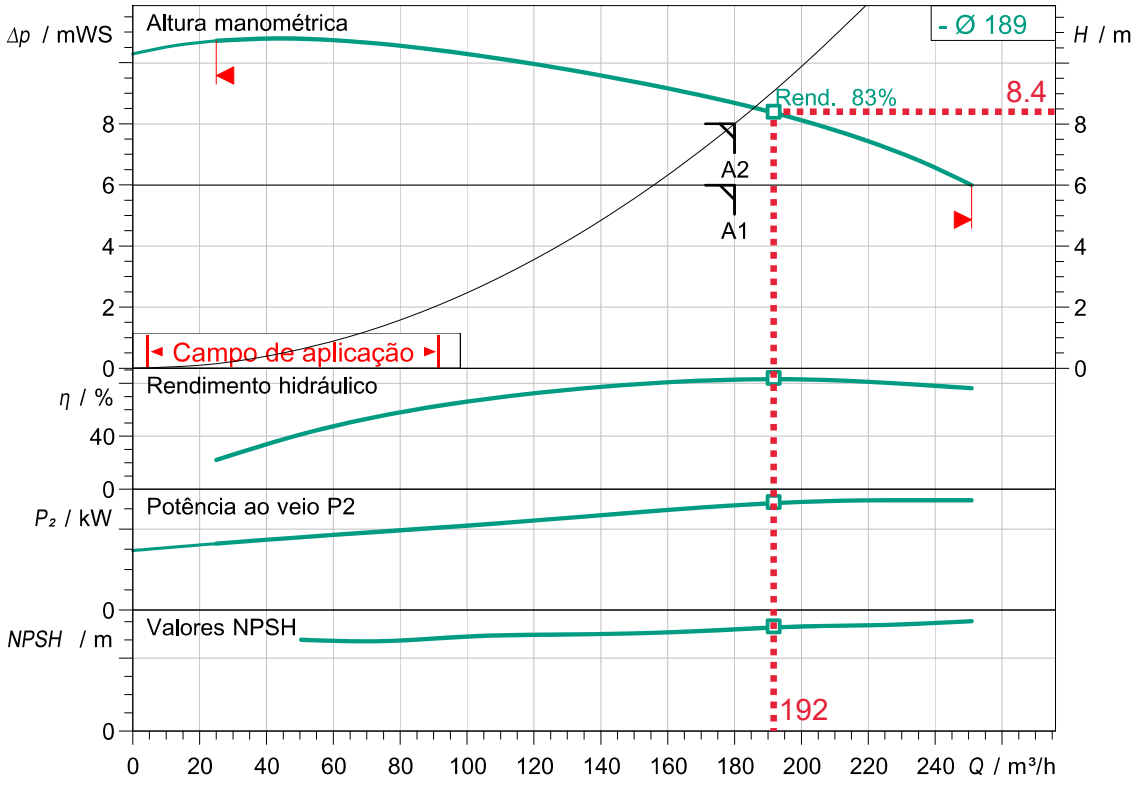

Figure 4.6: Characteristic curves of the pump CronoBloc-BL-E. Source: Wilo [60].

The n_{sP} obtained in Equation 4.8 for the second PAT – hereinafter PAT CronoBloc-BL-E – is higher in comparison to that obtained for the first one. In this case, as long as the pump was not selected but is available in the lab, the rotational speed could not have been chosen to reach higher efficiency values (Figure 2.11), which may result in a lower efficiency for the PAT.

For example, if a preliminary specific speed was initially assumed to be 40 for these head and flow values, as in the first case, the recommended rotational speed obtained would be around 855 rpm. This would lead to the closest commercially available value, which is 960 rpm – not 1450 rpm.

Table 4.5: Results obtained for C_H, C_Q, and C_η for the second PAT.

Author	C_H	C_Q	C_η
Barbarelli et al. [26]	1.166	1.432	–
Pérez-Sánchez et al. [31]	1.486	1.329	–
Gülich [27]	1.251	1.161	0.821
Stepanoff [34]	1.205	1.098	1.000
Sharma [35]	1.251	1.161	1.000
Alatorre-Frenk [36]	1.389	1.319	0.964
Yang et al. [41]	1.473	1.329	–
MEAN	1.317	1.261	0.946

$$\begin{aligned} H_{bT} &= 1.317 \times 8.40 = 11.07\,[m] \\ Q_{bT} &= 1.261 \times 192 = 242.17\,[m^3/h] \\ \eta_{bT} &= 0.946 \times 83\% = 78.5\% \end{aligned} \tag{4.9}$$

From a hydraulic power of 6.42 kW and a generator efficiency of 85% [30], the generated electrical power will be equal to 5.46 kW – which can be applied in Level 2 to supply the demanded power during office hours or as a supplement.

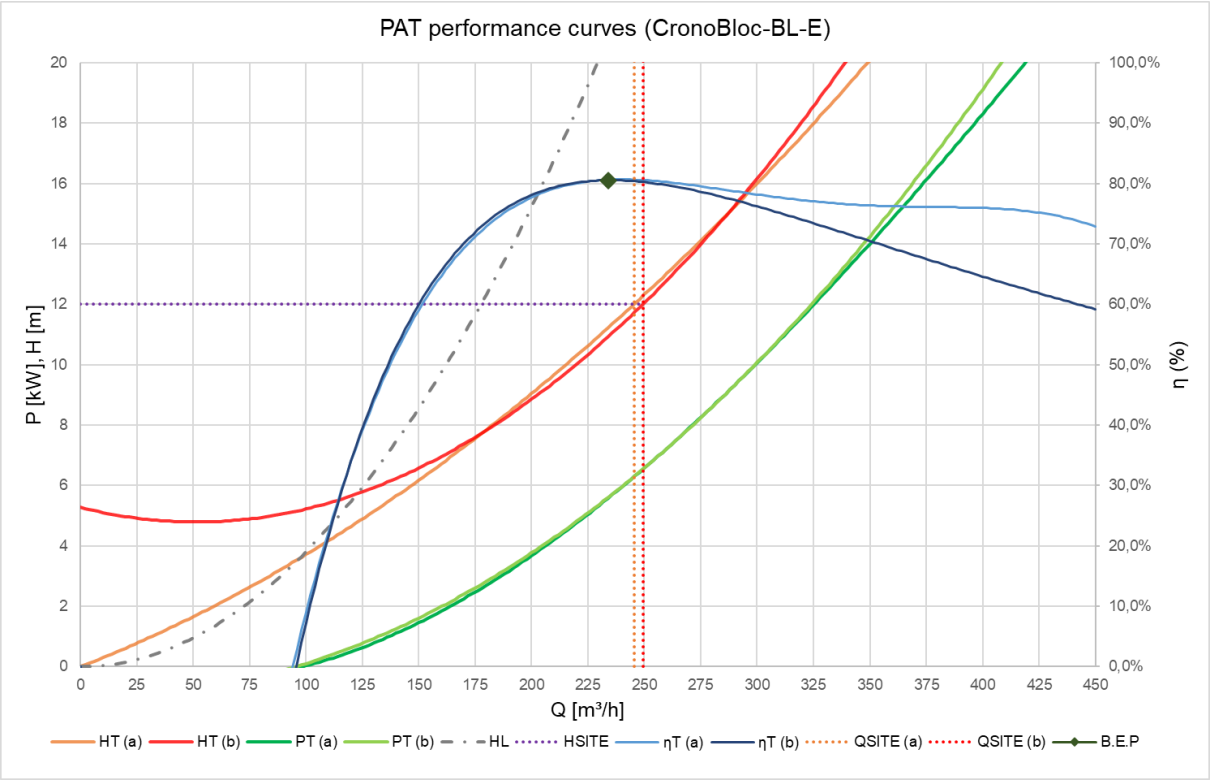

Figure 4.7: PAT performance curves for the pump CronoBloc-BL-E.

Table 4.6: Operating values for PAT CronoBloc-BL-E.

Method	$Q_T\ [m^3/h]$	$P_T\ [kW]$	$\eta_T\ [\%]$
Barbarelli et al. [26]	256.05	6.56	78.3
Pérez-Sánchez et al. [31]	251.78	6.28	78.6
MEAN	253.91	6.42	78.5

4.1.3 Grid connection

Since commercial pumps are generally sold with induction motors, the grid connection approaches must focus on induction generators. In the scope of this work, the main connection approach is through an electronic soft-starter. This simple solution relieves the large inrush currents and voltage drops implied by a direct connection. A basic scheme of this approach is shown in Figure 4.8.

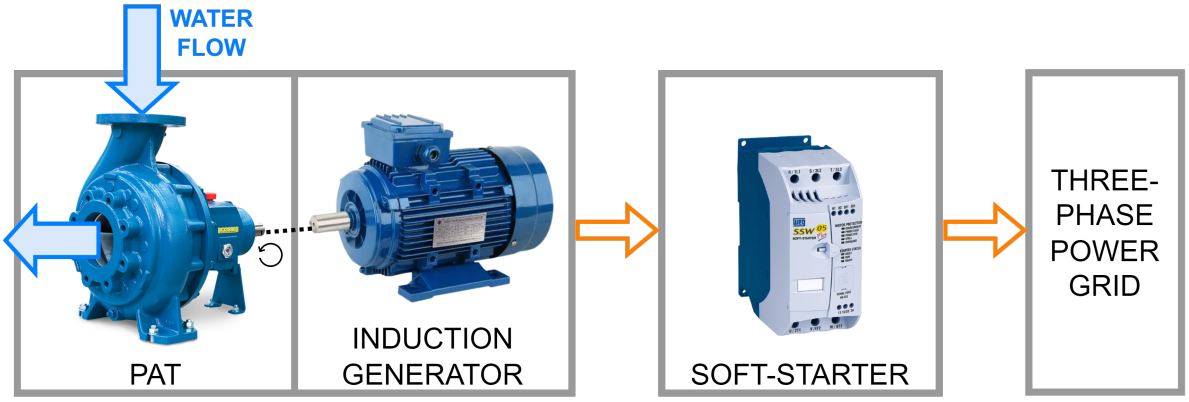

Figure 4.8: Basic scheme of the connection through a soft-starter.

In terms of starting, the smaller generator may not need the soft-starter as it has low power. Even so, this electronic device will be sized to meet the connection requirements for both PATs selected above, considering the respective power range. The soft-starter WEG Series 05 Plus – SSW-05 Plus – will be considered for such applications.

Figure 4.9 shows the front view of the device, where there are, e.g., motor enable and disable command, electronics power supply, protection enable, relay outputs, and setting trimpots – which configure pedestal voltage, acceleration and deceleration times,

and motor current.

The latter must be set as the ratio of the rated current of the device and the current of the driven motor, as it defines the machine protection and has a direct influence on overcurrent, overload, locked rotor, and phase loss protections [47]. Recommended setting values for applications such as hydraulic pumps are: pedestal voltage at 40%; acceleration time at 10 s; and no deceleration time [61].

A simplified soft-starter power and control diagram was previously shown in Figure 2.20. Here, other components will be added to complement this system. A new diagram is designed using a contactor, push-buttons, and the operation function relay to start and stop, as follows in Figure 4.10.

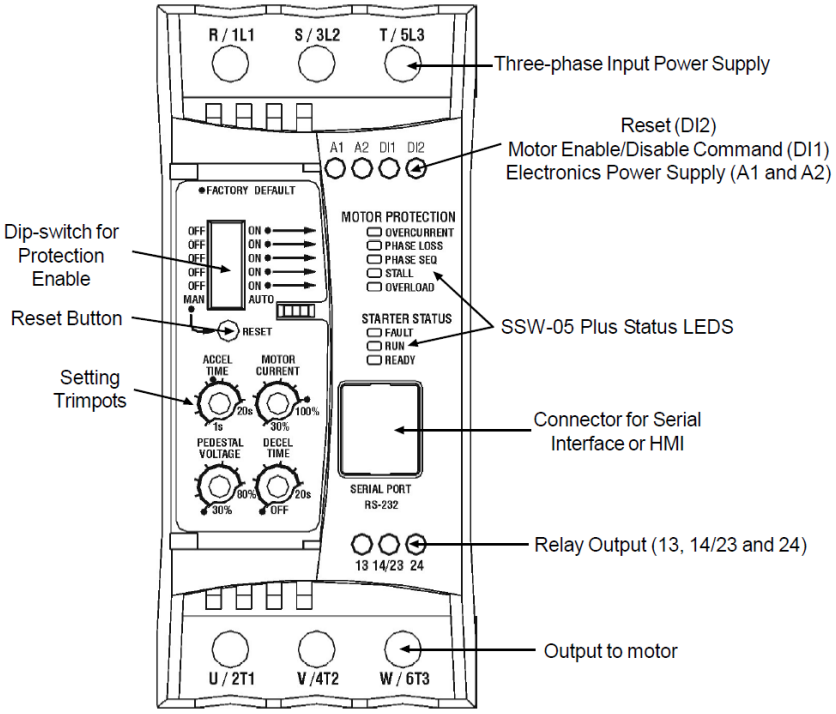

Figure 4.9: Front view of the SSW-05 Plus.

The relay used for the operation function closes its normally open switch (13-14/23) when the soft-starter receives an enable command and opens only at the end of the deceleration ramp or when the device receives the disable command. Thus, when the push-button S1 is pressed, an enable command is sent to digital input 1 DI1, closing the

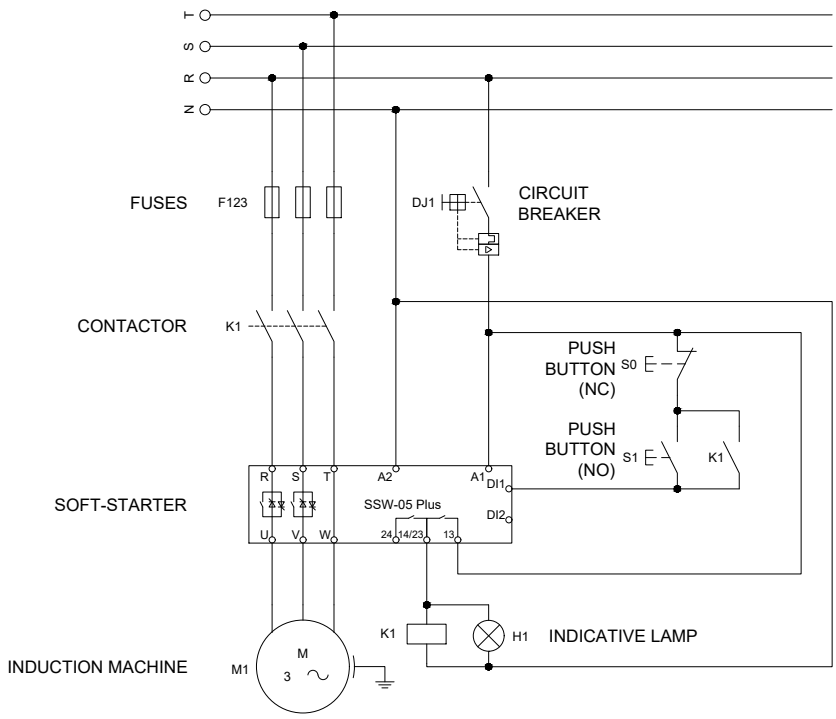

Figure 4.10: Power and control diagram using the SSW-05 Plus.

relay's normally open switch and energizing the contactor K1. Hence, the machine starts, and an indicative lamp H1 lights up. A seal-in contact from K1 keeps DI1 on. In order to stop the system, the push-button S0 must be pressed, interrupting the digital input's energy supply – and so de-energizing the contactor K1.

According to the manufacturer's manual [47], Tables 4.7 and 4.8 present the recommended specifications for the equipment shown in the diagram in Figure 4.10 to be applied for the two PATs.

Table 4.7: Recommended grid connection kit for PAT 080-065-165.

Item	**Description**	**Specification/Reference**
Soft-starter	SSW-05 Plus	10A (SSW-05.10)
F123	Fuses	D-16A
K1	Contactor	12A (CWM12)
M1	Induction machine	$<$ 3.7kW(5hp) @ 380-415V
DJ1	Circuit breaker	6A
H1	Indicative lamp	230V (Green)

Table 4.8: Recommended grid connection kit for PAT CronoBloc-BL-E.

Item	**Description**	**Specification/Reference**
Soft-starter	SSW-05 Plus	23A (SSW-05.23)
F123	Fuses	D-35A
K1	Contactor	25A (CWM25)
M1	Induction machine	$<$ 7.5kW(10hp) @ 380-415V
DJ1	Circuit breaker	6A
H1	Indicative lamp	230V (Green)

4.2 Results and Discussion

A small-scale pico-hydro system was conceived for the Bragança Ciência Viva Centre (CCVB) considering the implementation of two PATs, whose selection and performance prediction were carried out through an easy and reliable procedure, based on several authors.

Statistical correlations were arranged using the specific speed of the site for preliminary selection of the PAT, enhanced by further steps. Polynomials were used to calculate the performance curves of the PAT based on a wide pump sample. This method is helpful to allow a PAT selection in any situation where flow rate and head are available, predicting the parameters of the BEP of a selected PAT and its operating point.

Since the BEP of a PAT may not precisely coincide with the site parameters, an analysis of the operating points of these PATs is relevant. In the lack of flow and speed control systems, the operating point of the PATs is determined primarily by the available head, discounting losses. From Figure 4.4, one can note that the operating point of the PAT 080-065-160, obtained using the methods proposed by Barbarelli et al. [12] and Pérez-Sánchez et al. [31], is very close to the BEP – presenting practically equal hydraulic efficiency in both situations. This scenario resembles that presented in Figure 2.16(a).

According to Figure 4.7, the operating point of the PAT CronoBloc-BL-E is on the right of the BEP, characterized by the scenario presented in Figure 2.16(c). When this occurs, the efficiency decreases relative to that at BEP, but slowly and usually acceptably. It is worth noting that the maximum efficiency as a turbine is lower at BEP, given that

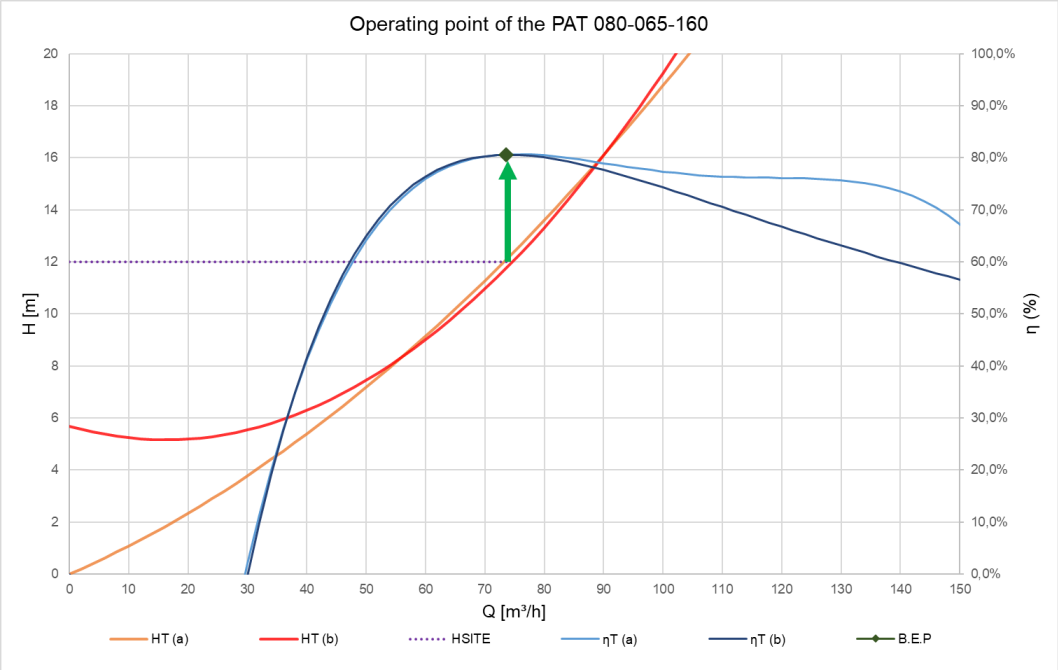

Figure 4.11: Operating point of the PAT 080-065-160.

the specific speed of this PAT is not between 30 and 50 – where efficiency reaches higher values. No significant efficiency drop was calculated for this operating point compared to the BEP efficiency. The worst-case scenario, when the operating point is on the left of the BEP, does not occur in these cases – observing any significant drop in efficiency.

These PATs, combined at three power levels, aim to meet different energy needs throughout the year and even during different times of the day. The main parameters obtained for each power level are described in Table 4.9 – where Q_T is the operating flow rate, P_O is the generated output power, and η_G is the global efficiency of the PAT set.

Table 4.9: Parameters of the three power levels.

Level	Q_T $[m^3/h]$	P_O $[kW]$	η_G [%]
1	73.88	1.63	68.5
2	253.91	5.46	66.7
3	327.80	7.08	67.1

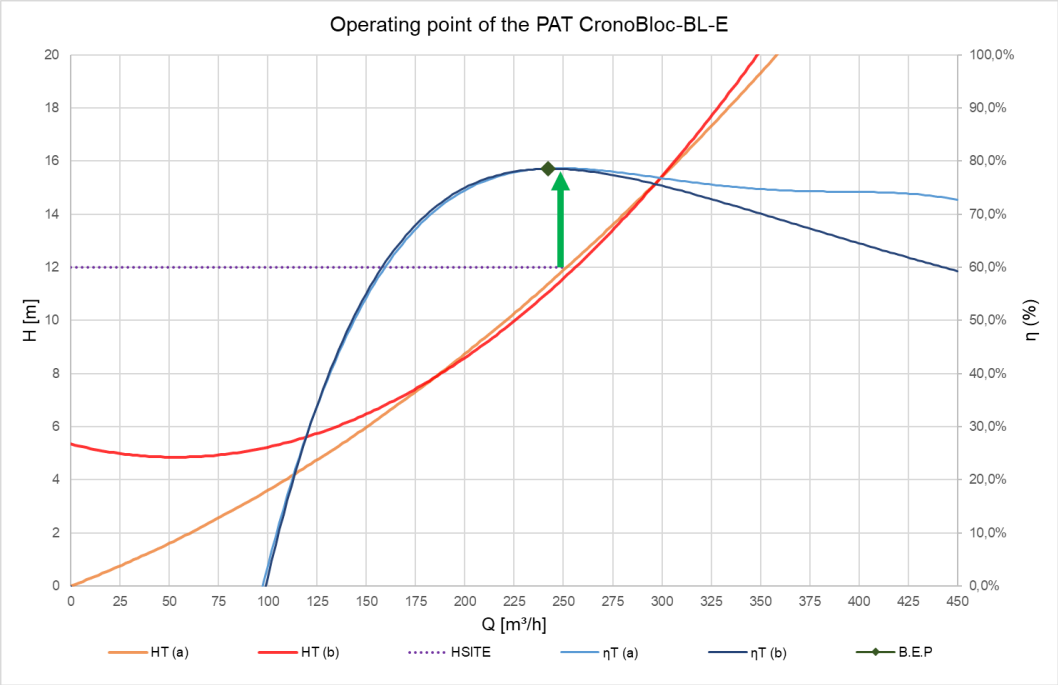

Figure 4.12: Operating point of the PAT CronoBloc-BL-E.

Although the efficiency of PAT is reported to be lower than that of conventional turbines, the payback from installing a PAT can have a period 5 times shorter [43]. Regarding further impacts of installing a PAT, it is important to highlight the environmental benefits that follow the economic analysis, usually called positive externalities. In addition to exploiting the hydroelectric potential of water streams, PATs are also appropriate solutions in other areas. In water distribution networks (WDN), for example, they can replace pressure-reducing valves (PRV), saving water while recovering energy at the same time [23].

Returning to the context of the work, operating conditions throughout the year must be analyzed. As mentioned, the dry summer months hinder a system operation all year, limiting it to 7 to 8 months [58]. Even so, this is an attractive solution as it generates energy 24 hours a day for a significant period – assuming the pump is mechanically prepared for this operation. At this location, abundant solar irradiance compensates for the reduced flow rate during summer and can be exploited in futures studies.

Different power levels must be utilized along the year, such as Figures 4.13, 4.14, and

4.15 suggest. The operating period of the system will be considered to be 226 days, approximately seven and a half months. In the winter, the system remains in operation with Level 3 for the entire period, considering that more available flow is available and so is the power demand. In the spring, the system also operates throughout the period but with different power levels. Level 1 is used during the entire first half of the season; during the second half, from 6 p.m. to 11 a.m., complemented by Level 2. In the summer, there is no operation, as in the first half of the autumn. Level 2 is employed from 6 p.m. to 11 a.m., and Level 3 from 11 a.m. to 6 p.m. in the second half of the autumn.

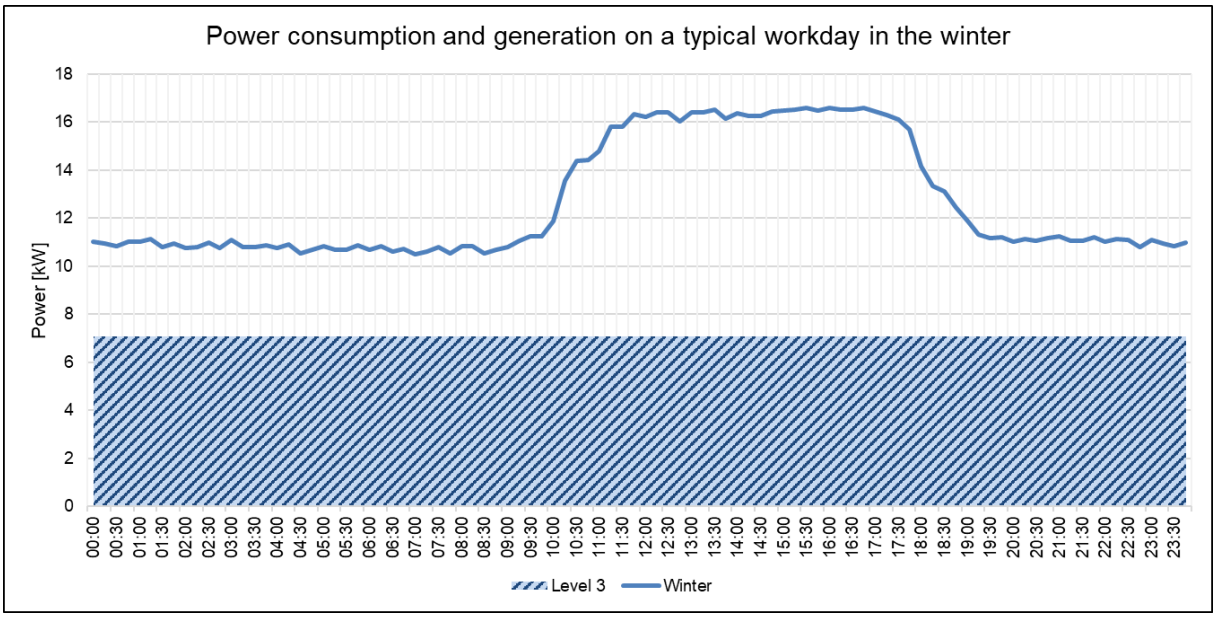

Figure 4.13: Power consumption and generation in the winter months.

A forecast of the system operation hours can be made based on these assumptions and, from this, a forecast of the energy generated, as presented in Tables 4.10 and 4.11.

The total power generation predicted in the scenarios described is 36,721 kWh, with a self-consumption quota of 100%, corresponding to 57% of the total consumption of 64,416 kWh observed over the one in the load diagrams. If only the months of operation are considered, this fraction becomes almost 80%. A maximum flow rate of 321.82 m^3/s is used when Level 3 is operating, about 54.6% of the flow rate demanded by the existing generator, during 25% of the operating period – winter and part of autumn.

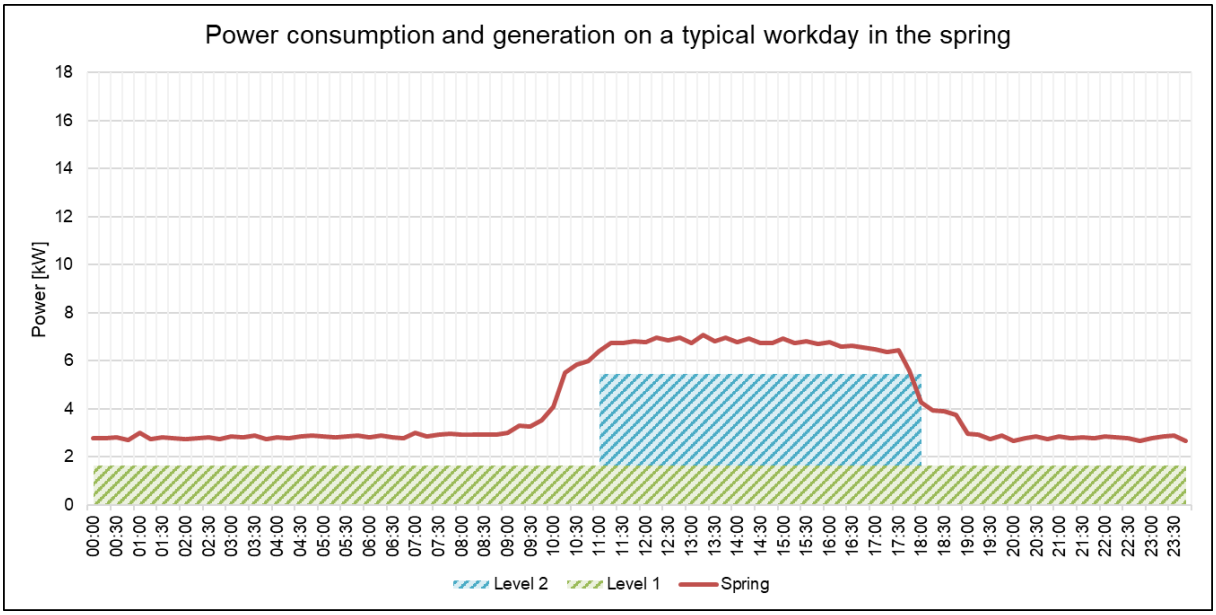

Figure 4.14: Power consumption and generation in the spring months.

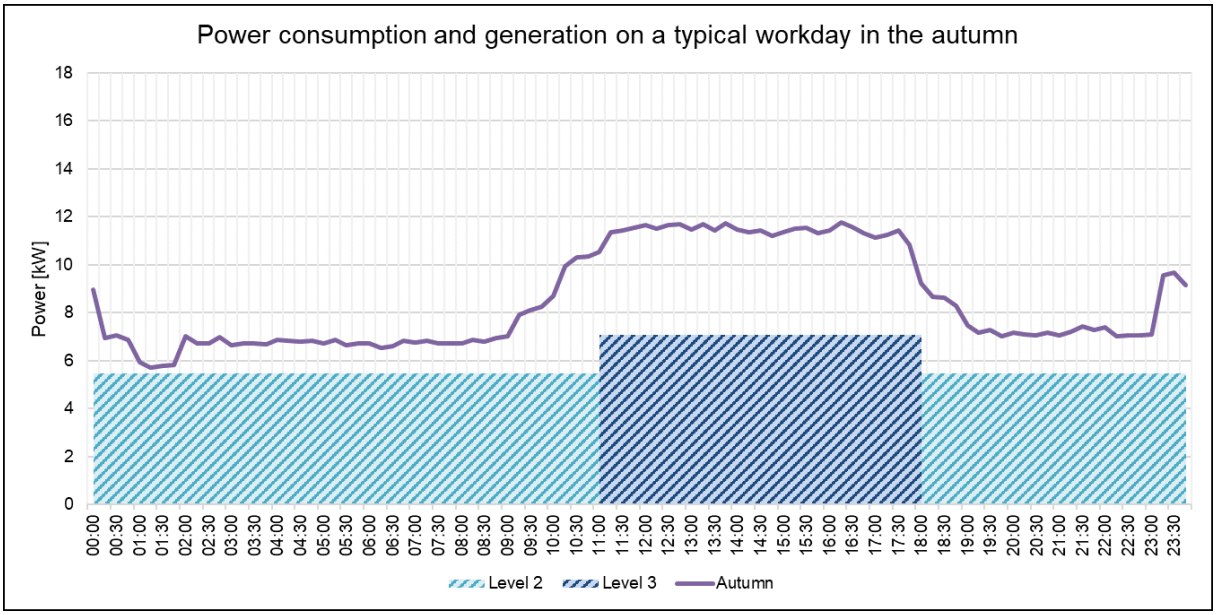

Figure 4.15: Power consumption and generation in the autumn months.

Table 4.10: Forecast of operation hours of the pico-hydro system for each power level.

Hours [h]	Winter	Spring	Summer	Autumn	Total
Level 1	0	3608	0	0	3608
Level 2	0	616	0	1496	2112
Level 3	2112	0	0	616	2112
Total	2112	4224	0	2112	8448

Table 4.11: Forecast of energy generation by the pico-hydro system.

Energy [kWh]	Winter	Spring	Summer	Autumn	Total
Level 1	0	5870	0	0	5870
Level 2	0	3362	0	8164	11525
Level 3	14961	0	0	4364	19325
Total	14961	9232	0	12527	36721

The electrical power generated by the system of 7.08 kW, when operating with the two PATs, is 9% higher than the hydroelectric potential preliminarily calculated at the beginning of Subsection 4.1.1, which considered the available flow as half of that demanded by the existing generator.

By comparison, a photovoltaic system of 24.5 kWp would be necessary for the same power generation for one year – considering an annual specific yield of 1,500 kWh/kWp for this site [17] –, representing an occupied roof area of approximately 120 m². Furthermore, considering the characteristic curve of PV generation, implementing a storage system would also be necessary for a high self-consumption quota. Still, as already mentioned, a photovoltaic system can be implemented in the future to complement the generation mainly in summer.

It is worth pointing out that the system proposed by this work is not a conventional hydropower system. Essentially, this pico-hydro system lacks flow control and also speed control. Moreover, weather conditions may have considerable differences throughout the years, as well as energy consumption. Excessive dirt, tailings, and organic matter in the riverbed may also compromise the water caption and suction, causing obstruction and

compromising the penstock.

For these reasons, it is a power generation system that requires constant monitoring and management. Based on the water flow and level of the river, influenced by environmental and climatic conditions, it may be necessary to modify the power levels in operation.

In the summer, for example, if there is sufficient flow in the river based on the rainfall regime, it may be possible to operate Level 1 for some period, as may happen in the early autumn. On the other hand, it may also be necessary to reduce power levels during the winter if this is a period with reduced rainfall.

As a system that operates on a self-consumption basis, its energy generation must track the energy consumption demand of the facility to maintain a higher self-consumption quota. In this context, monitoring consumption through energy bills alone does not provide sufficient information for analyzing and managing the pico-hydro system.

Thus, implementing an energy and power demand monitoring system in real-time would be an attractive resource to manage the generation system. Further automation tools could, for example, facilitate the start and stop of the hydraulic system, the connection of the generator to the power grid, or even the verification of disturbances or interruptions in the entire system.

4.3 Additional tests

As presented in Subsection 4.1.3, the grid connection strategy mainly considered in the scope of this work was through an electronic soft-starter. In addition, another innovative solution was initially tested in the lab, where a VFD is connected to the generator, exporting active power from its regenerative braking mode, which can be a cheaper solution for grid connection than bidirectional frequency converters. A PV inverter is also necessary to interface with the grid, connecting the DC bus of the VFD to the PV string inputs. Therefore, an emulating system for a PAT was implemented on the test bench, and then the new grid connection strategy was tested.

The static and dynamic behavior of the micro-hydro system at laboratory level requires a prime mover emulator to assist in the performance analysis of the overall system under variable conditions. For emulating a PAT, a 3 kW squirrel cage rotor induction motor controlled by a frequency converter was implemented. Since the hydro turbines present low-speed dynamics due to the high damping and inertia factor, it is possible to consider the speed control of the electric drive [20].

Also, a 1.5 kW induction machine was coupled to this and used in generator mode, interfacing with the power grid in different ways. This assembly is shown in Figure 4.16, and the technical data is presented in Table 4.12.

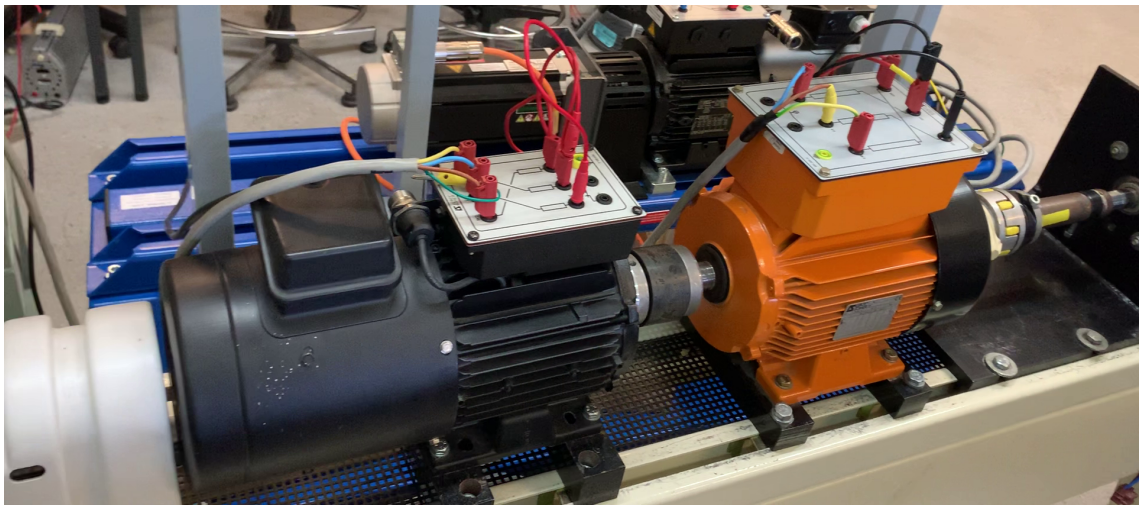

Figure 4.16: Emulation of the turbine on the test bench. On the right, the 3 kW induction motor simulating the PAT. On the left, on the same shaft, the 1.5 kW induction generator.

Table 4.12: Technical data of the induction machines.

Machine	**Manufacturer**	**Model**	**@400V(Y)-50Hz**			
			n **[rpm]**	P [kW]	I [A]	$cos\varphi$
Induction motor	Leroy Somer	3∼LSMV100L	1430	3	6.3	0.84
Induction generator	Leroy Somer	3∼LSVMV90L	1435	1.5	3.2	0.84

Firstly, the frequency converter was set to run the motor up to slightly above the synchronous speed. For this first test, the generator was connected directly to the power grid, and voltage and current values were measured and observed. When the speed of

the motor – and therefore the shaft – exceeded the synchronous speed, it was possible to notice that power was being exported to the grid. In order to emulate flow variations, different heads and flow rates, the power control of the primary unit was adopted, which results in a variable speed operation [50]. For such control, a 3 kW VFD, model ABB ACS 355, was implemented.

Rotational speed control can be performed in the generator using a second VFD, which allows working conditions at different speeds by changing the supply frequency [23]. Thus, operation under variable and seasonal conditions of head and flow is allowed. Figure 4.17 shows scenarios with different speed regulations, resulting in different operation points of a PAT.

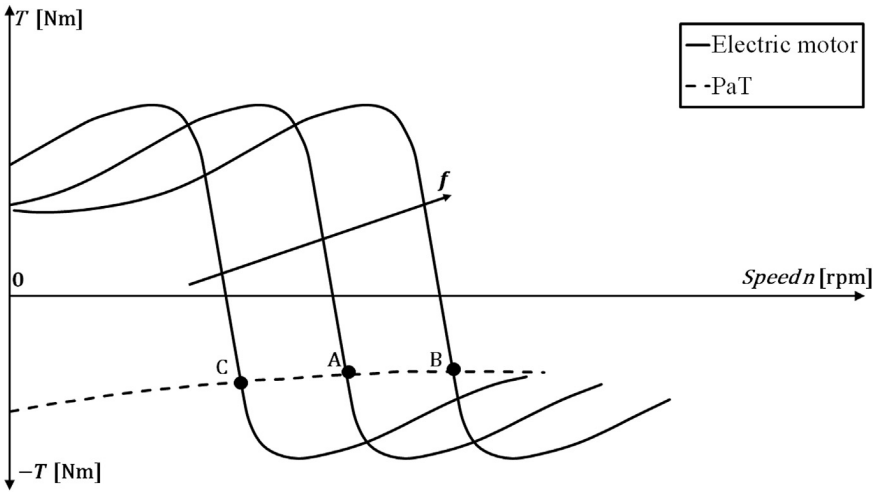

Figure 4.17: Speed regulation of a three-phase asynchronous motor by means of a VFD. Source: Stefanizzi et al. [23].

In order to export power to the grid, it was necessary to use a VFD that had the DC bus terminals accessible, which is why the model ABB ACS 600 was used. Generally, a VFD dissipates energy produced in the motor as the drive provides braking torque to either decelerate or stop the motor. For this, a brake chopper connects an external brake resistor to the DC bus voltage when the voltage exceeds its maximum limit. ABB ACS 600 does not have this system built in, so it is possible to implement it according to the specific requirements. The overvoltage fault occurs when DC bus voltage reaches 728 V.

Recent studies present simple and low-cost overvoltage protection circuits for this context [51, 62]. They are based on a step-down converter with a power IGBT and a free-wheeling diode to dissipate the energy in a power resistor, and the control is performed using the PWM controller TL494. In short, TL494 generates pulses when the DC voltage exceeds its maximum limit, triggering a IGBT and dissipating power to maintain the voltage in acceptable levels [51].

Adapting these solutions to the context of this work, the regenerative braking mode must export power from the DC bus to the grid through a PV inverter – instead of dissipating it in a power resistor. Essentially, the PV inverter would behave like a variable power resistor, adjusting it to absorb as much power as it could through its maximum power point tracking (MPPT) algorithm. A 2 kW PV inverter, model Solax Power X1-2.0-S-D(L), maximum DC voltage 450 V, was utilized in this case.

Nevertheless, this power export must not start at the normal DC bus voltage level as in motor operation, which is why a step-down converter is necessary. An additional protection circuit, as implemented by Scotta et al. [51], also dissipates energy in a power resistor at a higher voltage level, so as not to allow voltage values that could damage the VFD. Figure 4.18 presents a basic scheme of this system.

According to these instructions, the assembly in the lab was completed, as shown in Figure 4.19. Although proving to be an attractive and promising grid connection solution, replacing expensive bidirectional frequency converters and also enabling variable speed control, the operating dynamics of the PAT emulation system, the laboratory assembly scheme subject to noisy interference, and the MPPT algorithm of the PV inverter did not have sufficient compatibility.

While dissipating energy only in power resistors, the system worked. However, when connected to the inverter PV, it switched off immediately after the initial check procedure. The initial functioning of the MPPT algorithm may have caused current peaks in the system when switching it on. If this logic starts from testing the short-circuit current in a PV string, it may not work for a system with a different dynamic. If this logic starts by testing the short-circuit current in an PV string, it may not work for a system with

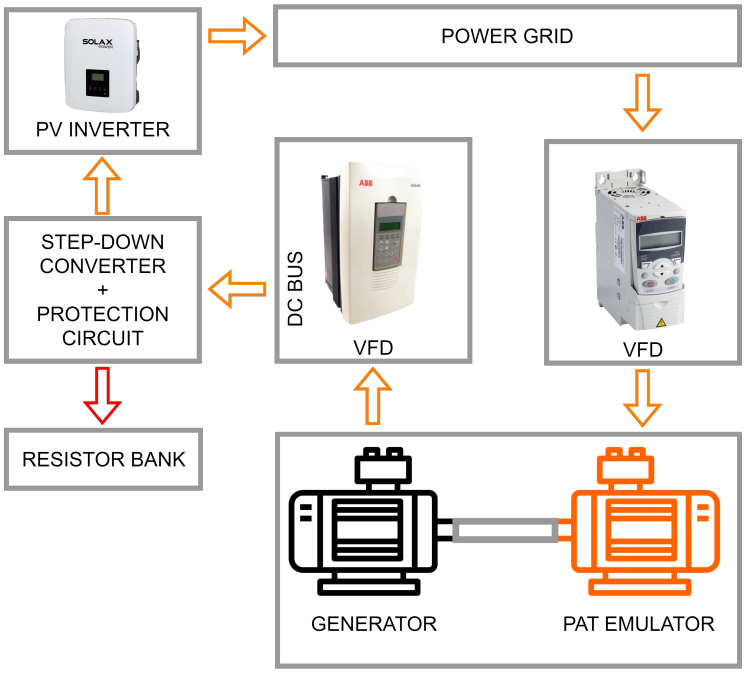

Figure 4.18: Basic scheme for connecting the PAT to the grid via VFD and PV inverter.

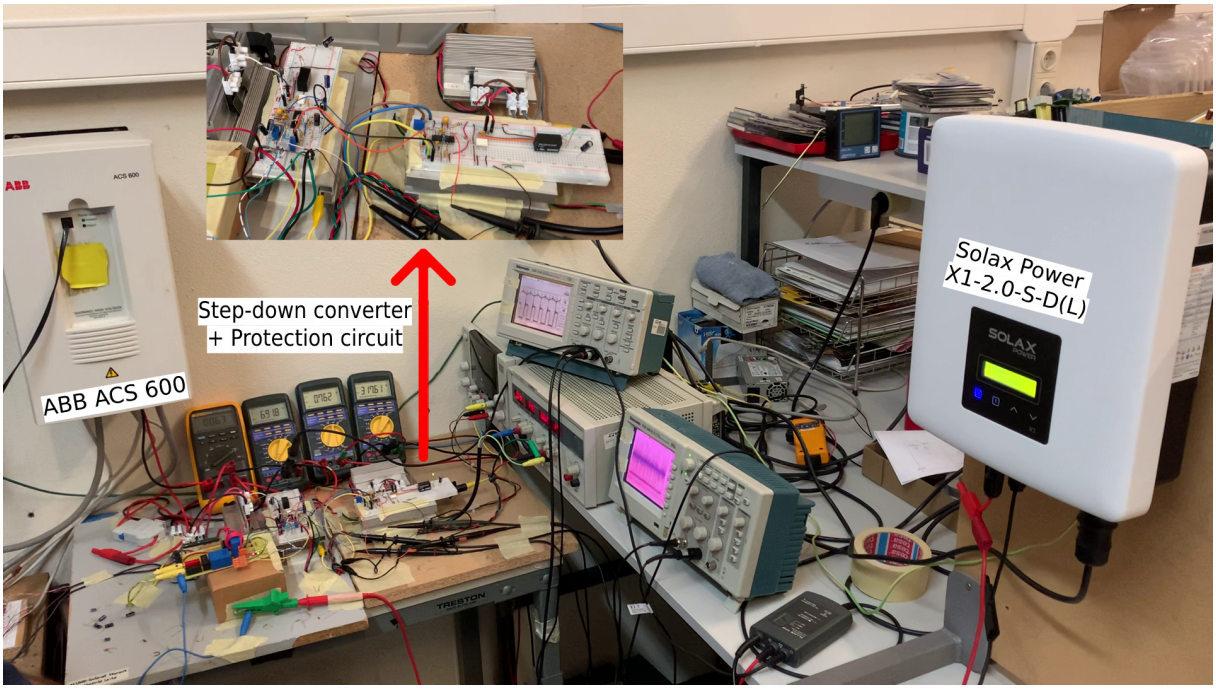

Figure 4.19: Assembling the new system in the laboratory.

different dynamics.

Chapter 5

Conclusion

After collecting consumption data and characterizing the site, a small-scale pico-hydro system was designed for the Bragança Ciência Viva Centre CCVB using pumps as turbines (PATs). The selection and performance prediction for the PATs were carried out through an easy and reliable procedure based on several authors and fully described in this work.

This procedure has the site parameters – available head and flow rate – as inputs, making it possible to select the equipment and predict its performance. Plus, the main grid connection approach adopted for the induction generators coupled to the PATs was through an electronic soft-starter, which is simple and effective.

In the scope of this work, a solution considering three power generation levels was proposed. Power levels of 1.63, 5.46, and 7.08 kW were arranged through different operational scenarios to obtain high shares of self-consumption. From the comparison of expected generation with consumption information for one year, 57% of the total consumption is reached. This amount can become almost 80% considering only the months of operation, which were considered to be approximately seven and a half months due to dry seasons – when the river flow decreases significantly.

Considering the current status of electricity demand and generation and rising electricity prices, small-scale renewable generation systems emerge as an attractive solution. In this context, small-scale pico-hydro systems have untapped potential in run-of-river plants for self-consumption. The procedure presented in this work can be applied to

other locations with available hydroelectric potential since it is based on a simple method – from experimental data and statistical analysis – and on mature technologies, which are widely available at competitive prices. This solution fills a void left by conventional hydraulic turbines in smaller capacities.

It is noteworthy that these pico-hydro systems require constant monitoring and management. That is why they, among other reasons, lack flow control and speed control, which differs from conventional hydropower systems. Variable weather conditions and energy consumption over the years also require power management. In addition, excessive dirt, tailings, and organic matter in the riverbed may also compromise the water caption and suction, causing obstruction and compromising the penstock.

Even so, applying PATs is an attractive solution since they are available for a wide range of head and flow rates and for various standard sizes, including spare parts, easy to install, low cost, less complex to operate, and mass-produced. Furthermore, coupled with induction generators allow more significant cost savings as their main advantages are simplicity, availability, price, robustness, and low maintenance.

In addition, preliminary tests were carried out in the lab for an innovative grid connection solution. A VFD was connected to the generator to export active power from its regenerative braking mode, with a PV inverter interfacing with the grid by connecting the DC bus of the VFD to the PV string inputs. A step-down converter and an additional protection circuit were also necessary to implement this system, which could configure a cheaper solution for grid connection than bidirectional frequency converters. An emulating system for a PAT was implemented on the test bench, and then the new grid connection strategy was tested. Although proving to be an attractive and promising solution, the operating dynamics of the PAT emulation system, the laboratory assembly scheme subject to noisy interference, and the MPPT algorithm of the PV inverter did not have sufficient compatibility. Consequently, additional research must be carried out in order to further develop this alternative.

5.1 Future work

This section contains suggestions on future lines of research related to the topic in question, intending to further improve and test the proposed solution:

- Implementation of a PAT and evaluation of its performance concerning the predicted operating curves, as well as its impact on the installation's power factor;
- Development of automation tools to system monitoring and management in real-time, prioritizing simple and cheap technologies. Such tools could, for example, start and stop the hydraulic system, connect and disconnect different power levels, or notify disturbances or interruptions;
- Design of a PV system as a supplement during dry summer months in the context of the CCVB;
- Further studies on the innovative grid connection solution using the regenerative braking mode of a VFD, as an alternative to bidirectional frequency converters, implementing a more robust and compatible emulating system.

Bibliography

[1] H. Ritchie and M. Roser, *Access to energy*, Accessed: 08 Aug 2022. [Online]. Available: https://ourworldindata.org/energy-access.

[2] A. S. Aidhen, S. Malik, and C. D. Kishanrao, "Performance of pump as turbine in pico hydro power generation," *International Journal of Mechanical and Production Engineering*, vol. 8, no. 6, pp. 10–15, Jun. 2020.

[3] A. G. Olabi and M. A. Abdelkareem, "Renewable energy and climate change," *Renewable and Sustainable Energy Reviews*, vol. 158, p. 112 111, 2022, ISSN: 1364-0321. DOI: https://doi.org/10.1016/j.rser.2022.112111.

[4] J. Osička and F. Černoch, "European energy politics after ukraine: The road ahead," *Energy Research & Social Science*, vol. 91, p. 102 757, 2022, ISSN: 2214-6296. DOI: https://doi.org/10.1016/j.erss.2022.102757. [Online]. Available: https://www.sciencedirect.com/science/article/pii/S2214629622002602.

[5] A. Lahimer, M. Alghoul, K. Sopian, N. Amin, N. Asim, and M. Fadhel, "Research and development aspects of pico-hydro power," *Renewable and Sustainable Energy Reviews*, vol. 16, no. 8, pp. 5861–5878, 2012, ISSN: 1364-0321. DOI: https://doi.org/10.1016/j.rser.2012.05.001. [Online]. Available: https://www.sciencedirect.com/science/article/pii/S1364032112003292.

[6] J. M. Guerrero *et al.*, "Distributed generation: Toward a new energy paradigm," *IEEE Industrial Electronics Magazine*, vol. 4, no. 1, pp. 52–64, 2010. DOI: 10.1109/MIE.2010.935862.

[7] V. Leite, "Design of a smart microgrid with small-scale hydro generation: A practical case study," *Revista Facultad de Ingeniería Universidad de Antioquia*, May 2022. DOI: 10.17533/udea.redin.20220577. [Online]. Available: https://revistas.udea.edu.co/index.php/ingenieria/article/view/345326.

[8] H. Europe, *Hydropower energy*, Accessed: 08 Aug 2022, 2020. [Online]. Available: https://hydropower-europe.eu/about-hydropower-europe/hydropower-energy/.

[9] A. S. Aidhen and P. H. Gaikwad, "Pump as turbine with induction generators in pico hydro for electrification of high terrain areas: A review," *International Journal of Current Engineering and Technology*, vol. 6, no. 5, pp. 1543–1548, Oct. 2016.

[10] O. Paish, "Micro-hydropower: Status and prospects," *Proceedings of The Institution of Mechanical Engineers Part A-journal of Power and Energy - PROC INST MECH ENG A-J POWER*, vol. 216, pp. 31–40, Feb. 2002. DOI: 10.1243/095765002760024827.

[11] S. Phuttarat, S. Somkul, C. Sirisamphanwong, and S. Ruangsinchaiwanich, "Experimental investigation of pump as turbine and induction generator for pico hydro power," *Journal of Renewable Energy and Smart Grid Technology*, vol. 14, no. 2, 2019.

[12] S. Barbarelli, M. Amelio, G. Florio, and N. Scornaienchi, "Procedure selecting pumps running as turbines in micro hydro plants," *Energy Procedia*, vol. 126, pp. 549–556, 2017, ATI 2017 - 72nd Conference of the Italian Thermal Machines Engineering Association, ISSN: 1876-6102. DOI: https://doi.org/10.1016/j.egypro.2017.08.282. [Online]. Available: https://www.sciencedirect.com/science/article/pii/S1876610217337888.

[13] W. Deprez, A. Dexters, J. Driesen, and R. Belmans, "Energy efficiency of small induction machines: Comparison between motor and generator mode," *ICEM*, vol. 269, Jan. 2006.

[14] D. Roberts, "Grid connection and technology-best practice and philosophy," *MorbenHydro*, 2008.

[15] V. Leite, Â. Ferreira, J. Couto, and J. Batista, "Compatibility analysis of grid-connected pico-hydro systems using conventional photovoltaic inverters," in *2016 18th European Conference on Power Electronics and Applications (EPE'16 ECCE Europe)*, 2016, pp. 1–9. DOI: 10.1109/EPE.2016.7695615.

[16] C. de Ciência Viva de Bragança, *Quem somos e associados*, Accessed: 28 Aug 2022. [Online]. Available: https://braganca.cienciaviva.pt/2235/quem-somos-e-associados.

[17] V. Leite, "Innovative smart microgrid integrating pico-hydro systems: The silk house museum," in 2020.

[18] H. Ritchie, M. Roser, and P. Rosado, *Renewable energy*, Accessed: 08 Aug 2022, 2021. [Online]. Available: https://ourworldindata.org/renewable-energy.

[19] R. Bansal, *Handbook of Distributed Generation: Electric Power Technologies, Economics and Environmental Impacts*. Springer International Publishing, 2017, ISBN: 9783319513430. [Online]. Available: https://books.google.pt/books?id=q09GDgAAQBAJ.

[20] A. Leite, J. Couto, Â. Ferreira, and J. Batista, "A practical approach for grid-connected pico-hydro systems using conventional photovoltaic inverters," Apr. 2016, pp. 1–6. DOI: 10.1109/ENERGYCON.2016.7513911.

[21] I. H. Association *et al.*, *Hydropower 2050: Identifying the next 850+ gw towards net zero, international hydropower association, 2020*.

[22] S. V. Jain and R. N. Patel, "Investigations on pump running in turbine mode: A review of the state-of-the-art," *Renewable and Sustainable Energy Reviews*, vol. 30, pp. 841–868, 2014, ISSN: 1364-0321. DOI: https://doi.org/10.1016/j.rser.2013.11.030. [Online]. Available: https://www.sciencedirect.com/science/article/pii/S136403211300779X.

[23] M. Stefanizzi, T. Capurso, G. Balacco, M. Binetti, S. M. Camporeale, and M. Torresi, "Selection, control and techno-economic feasibility of pumps as turbines in water distribution networks," *Renewable Energy*, vol. 162, pp. 1292–1306, 2020, ISSN: 0960-1481. DOI: https://doi.org/10.1016/j.renene.2020.08.108. [Online]. Available: https://www.sciencedirect.com/science/article/pii/S0960148120313537.

[24] B. J. Beecher, "Modern power station practice," in B. E. International, Ed., 3rd. Pergamon, 1991, vol. C, ch. 5, pp. 422–428, ISBN: 0-08-040513-4.

[25] W. P. T. Office, *Types of hydropower turbines*, Accessed: 09 Aug 2022. [Online]. Available: https://www.energy.gov/eere/water/types-hydropower-turbines.

[26] S. Barbarelli, M. Amelio, and G. Florio, "Using a statistical-numerical procedure for the selection of pumps running as turbines to be applied in water pipelines: Study cases," *Journal of Sustainable Development of Energy, Water and Environment Systems*, vol. N/A, Nov. 2017. DOI: 10.13044/j.sdewes.d5.0181.

[27] J. Gülich, *Centrifugal Pumps*. Springer London, Limited, 2008, ISBN: 9783540736943. [Online]. Available: https://books.google.pt/books?id=8kmdXwAACAAJ.

[28] J.-M. Chapallaz, P. Eichenberger, and G. Fischer, *Manual on pumps used as turbines*. Vieweg, Braunschweig, Germany, 1992.

[29] Andritz, *Andritz pumps and motors - products, systems, applications*, Accessed: 01 Sep 2022, 2017. [Online]. Available: https://www.andritz.com/resource/blob/34994/917811452770d8522c93906fda799759/hy-andritz-pumps-portfolio-en-data.pdf.

[30] KSB, *Efficiency class*, Accessed: 28 Aug 2022. [Online]. Available: https://www.ksb.com/en-global/centrifugal-pump-lexicon/article/efficiency-class-1116446?adlt=strict&toWww=1&redig=D7778585D4BA42A6A023783BB0546C5E.

[31] M. Pérez-Sánchez, F. J. Sánchez-Romero, H. M. Ramos, and P. A. López-Jiménez, "Improved planning of energy recovery in water systems using a new analytic approach to pat performance curves," *Water*, vol. 12, no. 2, 2020, ISSN: 2073-4441. DOI: 10.3390/w12020468. [Online]. Available: https://www.mdpi.com/2073-4441/12/2/468.

[32] A. A. Williams, "The turbine performance of centrifugal pumps: A comparison of prediction methods," *Proceedings of the Institution of Mechanical Engineers, Part A: Journal of Power and Energy*, vol. 208, no. 1, pp. 59–66, 1994. DOI: 10.1243/PIME_PROC_1994_208_009_02.

[33] S. M. Childs, "Convert pumps to turbines and recover hp," *Hydrocarbon Processingan Petroleum Refiner*, 1962.

[34] A. J. Stepanoff, "Centrifugal and axial flow pumps," *New York: John Wiley*, 1957.

[35] K. R. Sharma, "Small hydroelectric project-use of centrifugal pumps as turbines," *Kirloskar Electric Co., Bangalore, India*, 1985.

[36] C. Alatorre-Frenk and T. H. Thomas, "The pumps as turbines approach to small hydropower," *Word Congress on Renewable energy, Reading, UK*, 1990.

[37] J. W. Hancock, "Centrifugal pumps or water turbine," *Pipe Line News*, 1963.

[38] E. Schmield, "Series of centrifugal pumps in turbine operation (in german)," *Pumpentagung Karlsruhe*, 1988.

[39] K. M. Grover, "Conversion of pump to turbines," *GSA Inter Corp. Katonah, New York, USA*, 1980.

[40] H. P. Lewinsky-Kesslitz, "Pumps as turbines for small power plants (in german)," *Wasserwirtschaft*, 1987.

[41] S.-S. Yang, S. Derakhshan, and F.-Y. Kong, "Theoretical, numerical and experimental prediction of pump as turbine performance," *Renewable Energy*, vol. 48, pp. 507–513, 2012, ISSN: 0960-1481. DOI: https://doi.org/10.1016/j.renene.

2012.06.002. [Online]. Available: https://www.sciencedirect.com/science/article/pii/S0960148112003485.

[42] S. Fontanella, O. Fecarotta, B. Molino, L. Cozzolino, and R. Della Morte, "A performance prediction model for pumps as turbines (pats)," *Water*, vol. 12, no. 4, 2020, ISSN: 2073-4441. DOI: 10.3390/w12041175. [Online]. Available: https://www.mdpi.com/2073-4441/12/4/1175.

[43] A. Morabito and P. Hendrick, "Pump as turbine applied to micro energy storage and smart water grids: A case study," *Applied Energy*, vol. 241, pp. 567–579, 2019, ISSN: 0306-2619. DOI: https://doi.org/10.1016/j.apenergy.2019.03.018. [Online]. Available: https://www.sciencedirect.com/science/article/pii/S030626191930409X.

[44] S. Chapman, *Electric Machinery Fundamentals*. McGraw-Hill, 2012, ISBN: 9780071086172.

[45] M. Nikolič, D. Mršević, L. Ristić, đ. Čantrak, and N. Janković, "Induction machine driven pump applied as turbine in micro-hydro power plants," in *2021 6th International Symposium on Environment-Friendly Energies and Applications (EFEA)*, 2021, pp. 1–6. DOI: 10.1109/EFEA49713.2021.9406236.

[46] D. Wijaya, E. Firmansyah, S. Sarjiya, and M. I. Setyonegoro, "Grid connected-induction generator start-up sequence observation using laboratory simulator," 2015. DOI: 10.1109/ISGT-Asia.2015.7387139.

[47] WEG, *Installation and operation manual - ssw-05 plus*, 2002. [Online]. Available: https://static.weg.net/medias/downloadcenter/hde/h53/WEG-SSW05-user-manual-0899.5119-en.pdf.

[48] C. Greacen, R. Engel, and T. Quetchenbach, "A guidebook on grid interconnection and islanded operation of mini-grid power systems up to 200 kw," *Lawrence Berkeley National Laboratory*, 2013.

[49] L. Figueiredo, W. Maidana, and A. Leite, "Implementation of a smart microgrid in a small museum: The silk house," in Jan. 2020, pp. 121–134, ISBN: 978-3-030-38888-1. DOI: 10.1007/978-3-030-38889-8_10.

[50] G. Ribeiro, W. Maidana, A. Leite, and Â. Ferreira, "Grid connection approach for very small-scale pico-hydro systems using pv microinverters," Oct. 2019, pp. 2372–2376. DOI: 10.1109/IECON.2019.8926691.

[51] I. C. Scotta, W. Maidana, and V. Leite, "Overvoltage protection for grid-connected pico-hydro generation using photovoltaic inverters," en, *Revista Facultad de Ingeniería Universidad de Antioquia*, pp. 73–82, Jun. 2021, ISSN: 0120-6230. [Online]. Available: http://www.scielo.org.co/scielo.php?script=sci%5C_arttext&pid=S0120-62302021000200073&nrm=iso.

[52] B. H. B. Tangerino, "Power converters control for photovoltaic water pumping system," Ph.D. dissertation, Instituto Politécnico de Bragança (IPB), 2019.

[53] ABB, *Acs355 drives - user's manual*, 2020. [Online]. Available: https://library.e.abb.com/public/805f31a82d524d8aa8a750011e2cd001/EN%5C_ACS355%5C_UM%5C_E%5C_A5.pdf.

[54] ——, *Acs880-11 drives - hardware manual*, 2021. [Online]. Available: https://library.e.abb.com/public/50613c479ec8489ba19254aeaf368a70/EN%5C_ACS880-11%5C_HW%5C_G.pdf.

[55] C. de Ciência Viva de Bragança, *História e memória*, Accessed: 28 Aug 2022. [Online]. Available: https://braganca.cienciaviva.pt/2233/historia-e-memoria.

[56] G. Maps, *Centro de ciência viva*, Accessed: 28 Aug 2022. [Online]. Available: https://goo.gl/maps/eA719YeC4cyh4oYb6.

[57] EDP, *Tarifários*, Accessed: 28 Aug 2022. [Online]. Available: https://www.edp.pt/particulares/energia/tarifarios/.

[58] A. Leite, T. Figueiredo, T. Pinheiro, Â. Ferreira, and J. Batista, "Dealing with the very small: First steps of a picohydro demonstration project in an university campus," *Renewable Energy and Power Quality*, pp. 1305–1310, Apr. 2012. DOI: 10.24084/repqj10.683.

[59] KSB, *Characteristic curves booklet*, Standardised Water Pump / Thermal Oil and Hot Water Pump - 50 Hz, Jun. 2021.

[60] WILO, *Características técnicas bomba monobloco de rotor seco bl 125/185-5,5/4*, 2015.

[61] Siemens, *Equipment manual - sirius 3rw30 / 3rw40 soft starters*, Accessed: 01 Set 2022, Oct. 2018. [Online]. Available: https://support.industry.siemens.com/cs/attachments/38752095/Manual%5C_softstarter%5C_3RW30%5C_3RW40%5C_en-US.pdf?download=true.

[62] F. Peretti, "Otimização da energia produzida por sistemas fotovoltaicos de autoconsumo," Ph.D. dissertation, Instituto Politécnico de Bragança (IPB), 2020.